Global and Planetary Change 223 (2023) 104100

Contents lists available at ScienceDirect

Global and Planetary Change

journal homepage: www.elsevier.com/locate/gloplacha

Centennial-millennial scale ocean-climate variability in the northeastern Atlantic across the last three terminations

Harshit Singh [a], Arun Deo Singh [a,c,*], Ravi Tripathi [b], Pradyumna Singh [a,c], Komal Verma [a], Antje H.L. Voelker [d,e], David A. Hodell [f]

[a] Department of Geology, Banaras Hindu University, Varanasi - 221005, India.
[b] Geological Survey of India, Bengaluru, -560078, India.
[c] DST-Mahamana Centre of Excellence in Climate Change Research, Institute of Environmental and Sustainable Development, Banaras Hindu University, Varanasi - 221005, India.
[d] Divisão de Geologia e Georecursos Marinhos, Instituto Português do Mar e da Atmosfera (IPMA), Avenida Doutor Alfredo Magalhães Ramalho 6, Alges,1495-165, Portugal.
[e] CCMAR, Centro de Ciências do Mar, Universidade do Algarve, Campus de Gambelas, 8005-139, Faro, Portugal.
[f] Godwin Laboratory for Palaeoclimate Research, Department of Earth Sciences, University of Cambridge, Cambridge CB2 3EQ, United Kingdom.

ARTICLE INFO

Editor Name: Dr. Fabienne Marret-Davies

Keywords:
Atlantic Ocean
Iberian margin
IODP Site U1385
Planktic foraminifera
SST
Terminations
Heinrich stadials
Interglacial

ABSTRACT

Changes in Earth's orbital parameters pace the Pleistocene glacial-interglacial cycles, although considerable ambiguity still remains over the interaction of the internal climatic variables, such as ice-sheet instability and ocean circulation that allow transitions into and out of an interglacial. Here, we analyse high-resolution planktic foraminiferal proxies including sea-surface temperature (SST) based on an Artificial Neural Network (ANN) across the last three terminations (TI, TII and TIII) and the subsequent interglacials (Holocene, Marine Isotope Stages (MIS) 5e and 7e) from IODP Site U1385, SW Iberian Margin. To demarcate the stadials and interstadials, we combined the faunal and SST records with existing data at Site U1385 including log (Ca/Ti) and benthic and planktic $\delta^{18}O$. The composite records reveal details of the last three terminations in terms of abrupt climatic events occurring during these terminations. Termination I included three well-known climatic events: Heinrich stadial (HS)1, Bølling/Allerød (B/A) complex & Younger Dryas (YD). Termination II was interrupted by only HS11. Termination III included HS8.2 and HS8.1 which show more resemblance to HS2 (a stadial prior to TI) and HS1, suggesting the YD is a unique feature of the last deglaciation. Additionally, TI and TII reveal similar durations (~6 kyr) with rates of SST change (~1.5 °C/kyr to ~2.1 °C/kyr), whereas TIII represents a longer process (~10 kyr) with a relatively slow rate of SST change (~0.8 °C/kyr). The anatomy of stadials (HS1, HS2, HS11 & HS8.1) reveals a complex history ('W' shaped anatomy) with two or three cold phases sandwiching (a) brief warm event(s). The European ice-sheet melting possibly initiated the stadial cooling at the Iberian Margin followed by the mid-latitude summertime warming and the intermediate-depth water mass warming that probably induced the Laurentide ice-sheet melting resulting in the complex stadial pattern. Our records further reveal a major reorganization of the surface current system, oceanographic fronts and productivity conditions across these terminations. We also document broad similarities in the climatic evolution of Holocene, MIS 5e and 7e interglacials in terms of SST, surface productivity and current system. The long-term interglacial trends were superimposed by multiple brief cold events interrupting the Holocene (~11.3, 9.9, 8.2, 7.1, 5.5, 2.5 ka), MIS 5e (C28, C27, C27', C27a, C27b, C26, C26', C25), and MIS 7e (~238, 234, 231, 230 ka) interglacials. Integration of our records with benthic foraminiferal $\delta^{13}C$ records from the Iberian Margin and central North Atlantic suggest fluctuations in the deep water convection process (which in turn were influenced by the conditions in subpolar gyre) possibly resulted in the brief cold events interrupting the interglacials at the Iberian Margin.

* Corresponding author at: Department of Geology, Banaras Hindu University, Varanasi 221005, India
E-mail address: arundeosingh@yahoo.com (A.D. Singh).

https://doi.org/10.1016/j.gloplacha.2023.104100
Received 4 August 2022; Received in revised form 18 March 2023; Accepted 24 March 2023
Available online 26 March 2023

1. Introduction

During the Pleistocene, Earth's climatic system underwent cyclic fluctuations between glacial and interglacial conditions superimposed by millennial-scale variability (e.g. McManus et al., 1999; Jouzel et al., 2007; Barker et al., 2011). The transition interval from glacial to interglacial conditions was relatively rapid and is referred to as a deglaciation or termination. During deglaciations, rising mid to high latitudes boreal summer insolation initiated the melting of Northern Hemisphere ice-sheets, which delivered freshwater to the North Atlantic Ocean. This resulted in the short-term weakening of the Atlantic Meridional Overturning Circulation (AMOC) and the subsequent cooling of the Northern Hemisphere which is referred to as the terminal stadial event (Hodell et al., 2015). Consequently, the Intertropical Convergence Zone (ITCZ) shifted southwards and thereby displacing the South Atlantic subtropical gyre towards Antarctica. The southern shift of this gyre probably transported and strengthened the Southern Hemisphere westerlies resulting in the warming of Antarctica through oceanic heat transport, thereby triggering the outgassing of CO_2 through deep-water upwelling from the Southern Ocean reservoir (Anderson et al., 2009; Jiang and Yan, 2020; Pinho et al., 2021). The outgassing increased the atmospheric CO_2 concentrations by ~80 ppmv during the deglaciations and promoted warming to sustain the ensuing interglacial (e.g. Monnin et al., 2001; Denton et al., 2010; Shakun et al., 2012). Hence, the deglaciations represent very crucial intervals of near synchronous global and rapid climate change. Therefore, the study of deglaciations may provide a clear understanding of the Earth's climate system response to the rapidly changing background conditions.

The onset of interglacials is pre-conditioned by precession minima and insolation maxima (i.e., Northern Hemisphere summer occurring at perihelion). Millennial-scale temperature fluctuations during deglaciations and the subsequent interglacials are often expressed as temperature reversals. The deglacial temperature reversals are probably driven by, among others, ice volume, freshwater release, ocean circulation and greenhouse gas forcings, whereas the probable driving factors for the intra-interglacial temperature reversals are solar activity, volcanic eruptions and ocean circulation (e.g. Past Interglacials Working Group, 2015 and references therein). The structure of deglaciations are governed by feedback interactions between millennial and orbital variations (Barker and Knorr, 2021). For the events during the last two deglaciations and subsequent interglacials, the feedback mechanisms have been inferred from marine (Martrat et al., 2014; Jiménez-Amat and Zahn, 2015; Grunert et al., 2015; Tzedakis et al., 2018) and terrestrial proxy records (e.g. Grant et al., 2012; Moseley et al., 2015; Pickarski and Litt, 2017; Stoll et al., 2022) supported by modelling experiments (e.g. Toggweiler et al., 2006; Tschumi et al., 2011; Schmittner and Lund, 2015; Menviel et al., 2018). For Termination III (TIII) and MIS 7e, the feedbacks for the temperature reversals are poorly understood due to an insufficient number of high-resolution proxy records with well-constrained age models.

The sedimentary record recovered from IODP (International Ocean Discovery Program) Site U1385, off the SW Iberian Margin, is marked by high sedimentation rates (>10 cm/ka, Expedition 339 Scientists, 2013). Previous studies from this region exhibit signals of climatic events originating at the high-latitudes of both hemispheres (e.g. Shackleton, 2000; Vautravers and Shackleton, 2006; Martrat et al., 2007; Margari et al., 2014; Hodell et al., 2023). Site U1385 is located inside the northern limit of the Canary eastern boundary upwelling system and outside the southern- and easternmost limit of the ice rafted debris (IRD) belt making it an ideal site to record the signals of North Atlantic atmospheric and hydrographic systems (e.g. Bard et al., 2000; Salgueiro et al., 2010; Hodell et al., 2015; González-Lanchas et al., 2021). Because of its proximity to the continental margin, paleoclimatic records from this region permit detailed land-sea correlations needed to assess the role of the European Ice Sheet Complex (EISC) in global climate change (Toucanne et al., 2015; Kaboth-Bahr et al., 2018).

In this study, we reconstruct the past surface oceanographic changes at IODP Site U1385 on centennial-millennial timescale using planktic foraminiferal assemblages and SST records for the last three terminations (TI, TII & TIII) and the ensuing interglacials (Holocene, MIS 5e & 7e). The study identifies the sequence of climatic events interrupting the last three terminations based on their intensity, timing and duration, and the response of surface productivity and current systems to the changes in oceanographic fronts and SST variations. We also investigate the climatic progression of the interglacials following the last three terminations and evaluate the role of northern hemisphere climatic oscillations, AMOC and EISC in modulating these changes.

2. Oceanographic setting

Site U1385 (37°34.285′ N, 10°7.562′ W; 2578 m below sea level) was drilled on the continental slope of the SW Iberian Margin during the IODP Expedition 339 in the NE Atlantic Ocean (Fig. 1). The site is situated on a plateau known as the 'Promontorio dos Principes de Avis', which is raised above the Tagus abyssal plain and unaffected by turbidites (Hodell et al., 2015). Under modern conditions, the area under investigation is influenced by various water masses. The top-most layer (<100 m depth) is formed by surface waters originating in the North Atlantic. The Eastern North Atlantic Central Water (ENACW) comprises two components of water masses with different origins and properties (Fiúza et al., 1998). The $ENACW_{st}$ (100–250 m) is the warmer, shallower, saltier and nutrient-depleted component of subtropical origin formed along the Azores Front (AF) at ~35°N, while the $ENACW_{sp}$ (250–500 m) is colder, deeper, less saline and nutrient-laden component of subpolar origin formed north of 46°N due to winter cooling and deep convection (McCartney and Talley, 1982). The warm and saline Mediterranean Outflow Water (MOW) dominates the intermediate depths of the water column (500–1400 m; Ambar et al., 2002), whereas the cold and dense Northeast Atlantic Deep Water (NEADW) is the bottom most water mass at the study site (Fig. 1, Fiúza et al., 1998).

The surface hydrography of the SW Iberian Margin is characterized by a strong seasonal pattern (Fig. 1). Generally, the Azores High strengthens and shifts northward during the spring-summer seasons (April to September/October), promoting upwelling of subsurface water by the north-easterly trade winds (Fiúza, 1983). These upwelling filaments move up to 200 km offshore, potentially affecting productivity at the location of Site U1385 (Coste et al., 1986; Sousa and Bricaud, 1992). At the same time, an equator-ward flowing branch of the North Atlantic Current (NAC) i.e., the Portugal Current (PC) transports $ENACW_{sp}$ along the Iberian Margin (Fiúza, 1983). During the autumn and winter seasons (October to March/April), the Azores High weakens and moves southward causing the strengthening of the south-westerly winds, that intensifies the Iberian Poleward Current (IPC) (Teles-Machado et al., 2015). The IPC, being a branch of the Azores Current (AC) transports relatively warm, saline and nutrient-depleted water northwards, thus reducing primary productivity (Fig. 1, Peliz et al., 2005). The surface circulation at the examined site is also regulated by two oceanographic fronts: the thermal Subtropical Front and the Western Iberian Winter Front. The thermal Subtropical Front is closely associated with the eastern branch of the AC, which oscillates seasonally along 35–36°N, whereas, the Western Iberian Winter Front disconnects the cold waters of the PC from the warmer waters of the IPC along 38–40°N (Peliz et al., 2005).

3. Material and methodology

This study sampled the secondary splice that combines core sections of Holes U1385D and U1385E between 0.02 and 35.26 corrected revised meters composite depth (crmcd, Hodell et al., 2015). The sediment lithology is mainly pelagic/hemipelagic muds and clays with variable percentages of biogenic carbonates and terrigenous sediments (Expedition 339 Scientists, 2013). One cm thick slices of sediment were taken at

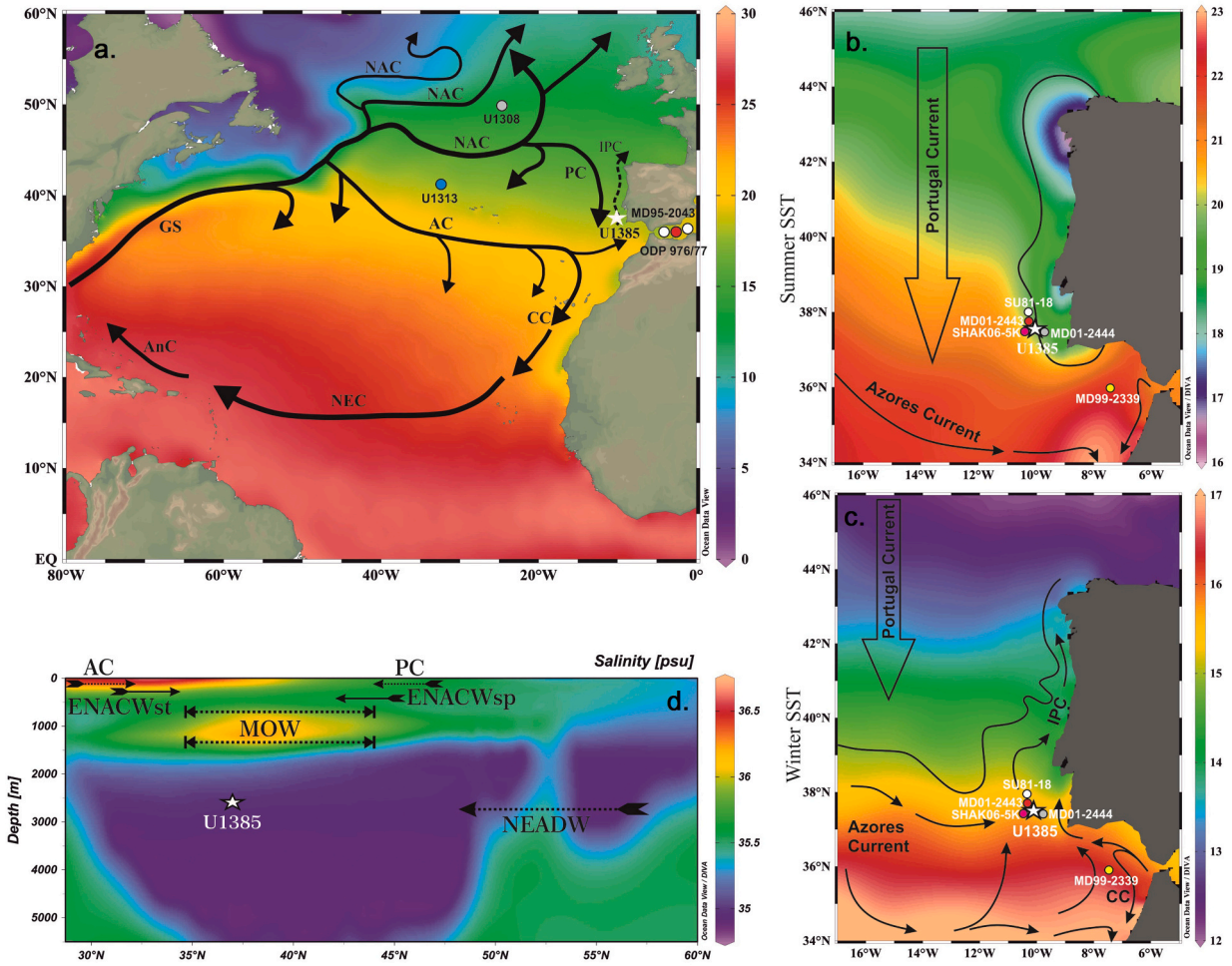

Fig. 1. (a) Map showing the location of IODP Site U1385 (star) in the SW Iberian margin and other core/sites discussed in the text (solid circle, IODP sites U1308/13, ODP sites 976/77, MD95–2043, MD01–2443/4, MD99–2339, SHAK06-5K & SU81–18). The coloured gradient represents modern mean annual (2018) distribution of SST based on World Ocean Atlas data (https://odv.awi.de/data/ocean/world-ocean-atlas-2018/) for the North Atlantic Ocean and off Portugal (b) during summer and (c) during winter seasons. Black arrows highlight the modern surface water circulation patterns. (d) Salinity (psu, colour shading) depth (m) latitude section and vertical structure of water masses in the North Atlantic Ocean (Map source is Ocean Data View software version 4.7.10; Schlitzer, 2014). PC=Portugal Current, AC = Azores Current, CC=Canary Current, IPC=Iberian Poleward Current, NEC=North Equatorial Current, AnC = Antilles Current, GS = Gulf Stream, $ENACW_{st}$ = Eastern North Atlantic Central Water (sub-tropical origin), $ENACW_{sp}$ = Eastern North Atlantic Central Water (sub-polar origin), MOW = Mediterranean Outflow Water and NEADW=North East Atlantic Deep Water.

2 cm intervals to obtain records of millennial-scale resolution.

A total of 484 sediment samples were used for the quantitative analyses of planktic foraminiferal assemblages. Sample processing was performed using the standard micropaleontological preparation techniques (e.g. Singh et al., 2015). About 5 g dried sediment of each sample was wet sieved through a > 63 μm screen. The dry residues >63 μm were weighed and dry sieved over a > 125 μm screen. Samples (>125 μm) were then split into sub-samples to obtain an approximate count of 300 planktic foraminifer specimens. For species identification, the taxonomic concepts of Kennett and Srinivasan (1983), Spezzaferri et al. (2015) and Schiebel and Hemleben (2017) were followed. Based on the census counts, relative abundance of each species was calculated.

We applied the ANN technique on planktic foraminiferal assemblages to estimate past SST at Site U1385, using the MARGO North Atlantic and Iberian Margin planktic foraminiferal database comprised of twenty six well known taxonomic categories (Kucera et al., 2005; Salgueiro et al., 2014). We extended the database to 1075 analogs using additional raw data from the NW Iberian Margin (Salgueiro et al., 2020). Modern SST values were extracted for the surface ocean at 10 m water depth from the World Ocean Atlas 1998. The MATLAB© software was used to reconstruct the annual-, summer- and winter-SSTs employing a back propagation neural network. For calibration, the database was split into three subsets: 80% for training and 10% for validation and 10% for testing. The methodology follows Kucera et al. (2005) and we used the same set of ten neural networks to provide ten different SST values of each component of annual-, summer-, and winter-temperature (see Kucera et al., 2005 for details). The averages of these ten SST reconstructions were used as the final SST values. The reconstructed SST values represent the upper water column temperature up to ~100 m rather than the surface (10 m), as it has been shown that planktic foraminiferal assemblages in some locations of the North Atlantic are more sensitive to subsurface temperatures than the usual depth (10 m) they are calibrated against (Telford et al., 2013).

For SST estimation in the North Atlantic region, the error is 1.14 °C for summer, 0.96 °C for winter and 0.96 °C for annual as predicted by Kucera et al. (2005). Additional error may arise due to the size disparity between the North Atlantic foraminiferal database (>150 μm) and our foraminiferal abundance records (>125 μm), which may result in an overrepresentation of the smaller species, viz. *Turborotalita quinqueloba*, *Turborotalita humilis*, *Globigerina rubescens* and *Globigerinoides tenellus*. In our record, *T. humilis* (~1.0%), *G. rubescens* (~1.2%) and *G. tenellus* (~0.03%) show rare and sporadic occurrences throughout the study

interval. Additionally, a study from the Arctic Ocean by Husum and Hald (2012) indicates that *T. quinqueloba* abundance compares well in both >150 μm and > 125 μm size fractions. This is consistent with previous investigations from the SW Iberian Margin that show average *T. quinqueloba* abundances of 7–10% for the time interval of the present study (e.g. Voelker and de Abreu, 2011), which compares well with our result (8.4%). The estimated error arising from the size disparity is minimal (0.26 °C).

Past changes in surface hydrography, frontal migrations and productivity fluctuations can be reconstructed using abundance variations of specific planktic foraminiferal species/groups (e.g. Cayre et al., 1999; de Abreu et al., 2003; Vautravers and Shackleton, 2006; Singh et al., 2015). The abundance records of *Neogloboquadrina pachyderma* and *T. quinqueloba* provide ample evidence of meridional shifts of polar/sub-polar fronts through time (e.g. Vautravers and Shackleton, 2006; Voelker et al., 2009; Singh et al., 2015). *N. pachyderma* is associated with the cold surface waters of high-latitudes and prefers a temperature range of −1 to 8 °C with an optimum temperature of 2 °C (Bé and Tolderlund, 1971; Johannessen et al., 1994; Pflaumann et al., 2003). Earlier studies have shown that the abundance of *N. pachyderma* is a reliable proxy for recognizing southern shifts of the polar front towards the Iberian Margin during the glacial stages (e.g. Bond et al., 1992; Vautravers and Shackleton, 2006; Eynaud et al., 2009; Singh et al., 2015). *T. quinqueloba* prefers slightly warmer conditions (1–21 °C) than *N. pachyderma* and proliferates today in Arctic Front waters with temperatures <12 °C. *T. quinqueloba* is abundant in the transitional domains of the polar water masses, and is regarded as a sub-polar species (Bé and Tolderlund, 1971; Pujol, 1980; Johannessen et al., 1994; Fronval et al., 1998). We used relative abundances of *N. pachyderma* and *T. quinqueloba* to trace the influence of polar/sub-polar water masses at Site U1385.

The tropical-subtropical mixed-layer species (*Globigerinoides ruber*, *Trilobatus sacculifer* plexus, *Globigerinella siphonifera*, *G. rubescens*, *Globigerina falconensis*, *Orbulina universa* and *Pulleniatina obliquiloculata*) grouped as warm water species (Vautravers et al., 2004) is a proxy for the IPC presence at the examined site, as living counterparts of these species show strong affinity to the warm surface waters of the AF (Schiebel and Hemleben, 2000; Schiebel et al., 2001; Storz et al., 2009). *Globorotalia inflata* and *Neogloboquadrina incompta* show strong affiliation to temperate conditions of the North Atlantic Transitional Waters (e.g. Ottens, 1992; Pflaumann et al., 1996; Chapman, 2010). We grouped them together to reconstruct the PC influence (Vautravers and Shackleton, 2006; Salgueiro et al., 2008; Singh et al., 2015). *Globigerina bulloides* and *Globigerinita glutinata* have strong preferences for the nutrient-laden upwelling environments of the eastern North Atlantic Ocean (Salgueiro et al., 2008; Wilke et al., 2009). *G. bulloides* is a well-established upwelling indicator and proliferates in highly productive coastal and open ocean upwelling areas (e.g. Kroon and Ganssen, 1988; Thunell and Sautter, 1992; Schiebel et al., 2001). *G. glutinata* is an opportunistic species which feeds on diatoms and prefers well-mixed nutrient-rich waters (Schiebel and Hemleben, 2000; Schmuker and Schiebel, 2002; Olson and Smart, 2004). We used abundances of *G. bulloides* in combination with *G. glutinata* to trace the past surface productivity and nutrient condition at the study site.

The age model of the examined sediment section is developed by the correlation of log (Ca/Ti) record (which reflects variations in % $CaCO_3$) of Site U1385 with log (Ca/Ti) record of adjacent cores (MD01–2443/44) having well-developed age models (see Age_Depth_GreenSyn age model in Hodell et al., 2015 for details). To further refine our age model for MIS 5e, we adopted the well-defined age model of core MD01–2444 (see Tzedakis et al., 2018 for details) by stacking and correlating the SST (this study) and planktic $\delta^{18}O$ (Hodell et al., 2015) records of the two cores (Supplementary Figs. S1 & S2). Holocene chronology of our annual SST record is compared with core MD95–2043 to confirm the robustness of the adopted age model (Alboran Sea, Cacho et al., 1999, Supplementary Fig. S3). The present study focuses on three separate time intervals: the last 25 ka (TI to Holocene), 115–140 ka (TII to MIS 5e) and 228–252 ka (TIII to MIS 7e). The estimated average temporal sampling interval of the proxy records is 151 years with respective resolutions of 121 for the last 25 ka, 192 for the interval 115–140 ka and 162 years for 228–252 ka. The MIS sub-stages were delineated following Railsback et al. (2015) and other studies from the Iberian and Mediterranean regions (e.g. Martrat et al., 2007, 2014; Hodell et al., 2015).

Stadials and interstadials encountered in this study were identified using planktic foraminiferal assemblages, ANN-based SST, log (Ca/Ti) and planktic (*G. bulloides*) and benthic (*Cibicidoides wuellerstorfi*) $\delta^{18}O$ records (Hodell et al., 2015; Hodell et al., 2023) of Site U1385. Sharp decreases in log (Ca/Ti) and SST values with increase in polar/sub-polar planktic foraminiferal species and high $\delta^{18}O$ values demarcate the stadials, whereas prominent increases in log (Ca/Ti) and SST values with corresponding decrease in polar/sub-polar planktics and low $\delta^{18}O$ values demarcate the interstadials. The stadials interrupting TIII were named HS8.2 and HS8.1 following Channell et al. (2012) and Hodell et al. (2023). Detailed chronologies of the climatic events documented in this study are presented in Table 1. The brief cold events interrupting the Holocene, MIS 5e & 7e interglacials were identified from the reconstructed SST record using the 'findpeaks' tool in the MATLAB© software by defining the 'MinPeakHeight' to be greater than the error value of the annual SST data (~1.22 °C) and the 'MinPeakDistance' to be greater than the average duration of the events (0.5 kyr).

4. Results

4.1. Planktic foraminiferal assemblages

A total of 31 planktic foraminiferal species are recorded from the examined samples. The most abundant species, accounting on average > 90% of the total planktic foraminiferal populations are: *G. bulloides* (~25.6%), *N. incompta* (~22.9%), *G. glutinata* (~10.7%), *G. inflata* (~8.2%), *T. quinqueloba* (~8.4%), *G. ruber* (~5.4%), *N. pachyderma* (~3.9%), *Globorotalia scitula* (~3.2%), *Globorotalia truncatulinoides* (~1.6%), *O. universa* (~1.2%) and *G. falconensis* (~1.3%). Other species show sporadic occurrences including *P. obliquiloculata* (~0.01%), *T. sacculifer* plexus (~0.7%), *Globorotalia hirsuta* (~0.2%), *Globorotalia crassaformis* (~0.1%), *G. siphonifera* (~1.0%), *T. humilis* (~1.0%), *G. rubescens* (1.2%) and *G. tenellus* (0.03%). The faunal assemblages comprise varied species/groups characterizing polar, sub-polar, transitional and subtropical water masses and species associated with high-nutrient conditions of the NE Atlantic Ocean. Temporal variations in relative abundances of ecologically significant planktic foraminiferal species used in the present study are shown in Fig. 2.

The polar species, *N. pachyderma* is one of the quantitatively significant species of the faunal record showing large variation in its abundance (50.8% to 0%) with maxima during the stadials and minima during the interstadials/interglacials. Maximum abundance of this species is associated with Heinrich stadial (HS) 1 (Fig. 2). *T. quinqueloba* is another important cold water species and its abundance varies from 39.8% to 0%. This species generally follows the pattern of *N. pachyderma* abundance variation; however, its abundance increases during the late part of MIS 5e and 7e interglacials. Nevertheless, both species show abundance peaks during stadials: Younger Dryas (YD), HS1, HS2, HS11, HS8.1 and HS8.2 (Fig. 2). The species associated with the PC (*N. incompta* and *G. inflata*) show patterns of variation opposite to *N. pachyderma* and *T. quinqueloba* with high abundances during interstadials/interglacials and low abundances during stadials. The abundance of *N. incompta* varies between 54% and 1.5%, whereas *G. inflata* ranges from 30% to 0% (Fig. 2). *G. bulloides* is the most abundant planktic species (on average) and its abundance ranges between 50% and 6% with greatest numbers during the interglacials, especially the Holocene. Along with a general decrease in its abundance pattern, we notice brief intervals of high abundance within the stadials YD, HS1, HS2, HS11 and HS8.2 and prominent increase during the HS8.1. The abundance of *G. bulloides* decreases during the interstadials

Table 1
Minimum, maximum and mean values of annual, summer and winter SST with SST gradient for the events documented at IODP Site U1385 along with their durations.

Interval	Event	Age range (ka)	SST gradient (°C/kyr)	Annual SST (°C) ±1.22 °C			Summer SST (°C) ±1.40 °C			Winter SST (°C) ±1.22 °C		
				Min.	Max.	Mean	Min.	Max.	Mean	Min.	Max.	Mean
	HS2	25–23.2		9.8	16.9	13.5	12.4	19.3	16.0	8.0	14.7	11.6
Termination I	HS1	17.2–15	~2.1	5.8	15.6	9.8	8.2	18.1	12.3	3.7	13.7	8.0
	B/A	15–12.5		14.9	17.7	16.3	17.5	20.1	18.9	12.6	15.4	14.0
	YD	12.5–11.6		11.0	16.8	13.1	13.5	19.4	15.5	9.0	14.5	11.2
Termination II	HS11	135.5–129.5	~1.5	10.1	14.6	12.3	12.5	16.8	14.8	8.4	12.7	10.4
	HS8.2	249.5–247.5		10.3	14.6	12.0	12.9	17.5	14.7	8.5	12.2	9.9
Termination III	Interstadial	247.5–243	~0.8	13.0	17.8	15.8	16.1	20.5	18.8	10.7	15.4	13.3
	HS8.1	243–239.5		11.0	17.0	13.2	13.7	19.5	15.9	9.1	14.9	11.0
	Early	11.6–8		15.8	19.0	17.8	18.1	21.4	20.1	13.7	16.8	15.6
Holocene	Middle	8–5		17.3	19.3	18.3	19.5	21.9	20.6	15.3	16.9	16.2
	Late	5–1	~0.3	17.1	19.0	17.9	19.2	21.5	20.2	15.2	16.9	15.8
Holocene		11.6–1		15.8	19.3	18.1	18.1	21.9	20.3	13.7	16.9	15.9
	Early	129.5–127		15.0	19.3	17.7	17.1	21.8	20.3	13.2	17.0	15.4
MIS 5e	Middle	127–120.5		14.7	18.1	16.9	17.6	20.7	19.5	12.3	16.0	14.8
	Late	120.5–115	~0.4	15.6	17.9	16.8	18.2	20.7	19.4	13.5	15.8	14.6
MIS 5e		129.5–115		14.7	19.3	17.1	17.1	21.8	19.7	12.3	17.0	14.9
	Early	239.5–236.5		16.1	18.2	17.0	19.0	20.9	19.9	13.6	16.0	14.5
MIS 7e	Middle	236.5–234		16.6	19.1	17.9	19.9	22.4	21.0	13.9	16.6	15.3
	Late	234–230.5	~0.6	14.3	17.0	15.8	17.4	20.1	18.8	11.8	14.5	13.3
MIS 7e		239.5–230.5		14.3	19.1	16.7	17.4	22.4	19.7	11.8	16.6	14.2

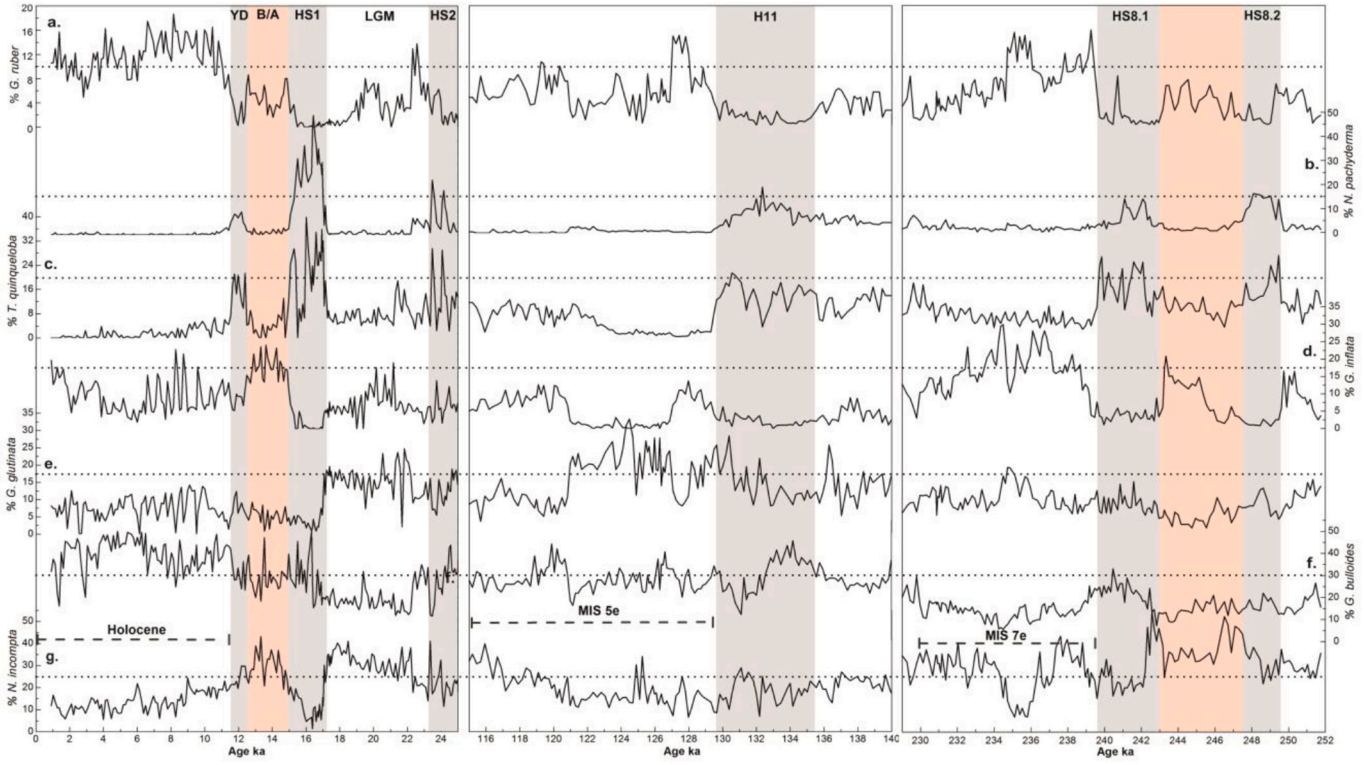

Fig. 2. Temporal variations in relative abundances of selected planktic foraminiferal species encountered in the present study: (a) *G. ruber*, (b) *N. pachyderma*, (c) *T. quinqueloba*, (d) *G. inflata*, (e) *G. glutinata*, (f) *G. bulloides* and (g) *N. incompta*. Vertical grey bars mark the stadials: YD, HS1, HS2, HS11, HS8.2 and HS8.1 whereas the pink bars mark the interstadials: B/A & TIII interstadial. Horizontal dotted lines are added for visual aid only. (For interpretation of the references to colour in this figure legend, the reader is referred to the web version of this article.)

interrupting the terminations (Fig. 2). The abundance of *G. glutinata* varies from 32.8% to 0% with maxima during the interglacials. This species shows abundance increases during YD, HS11, HS8.1 and HS8.2 and declines during HS1 and HS2. The abundance of *G. glutinata* increases during the Bølling/Allerød (B/A), whereas it decreases during the interstadial interrupting the deglaciation of MIS 8 (Fig. 2). The abundance of the warm water species group (*G. ruber*, *T. sacculifer* plexus, *G. siphonifera*, *G. rubescens*, *G. falconensis*, *O. universa*, *P. obliquiloculata*) remains generally <20% except during the Holocene period. Its abundance varies from 37.5% to 0% with peak abundances during the interstadials and interglacials, while minimum abundances occur during the stadials (Fig. 3).

4.2. ANN-based SST variations

The annual SST record generally follows the log (Ca/Ti) profile of the Site U1385 (Fig. 3). The terminations (TI, TII & TIII) are characterized by large-amplitude annual SST variations from ~8.8 to 13.5 °C. The

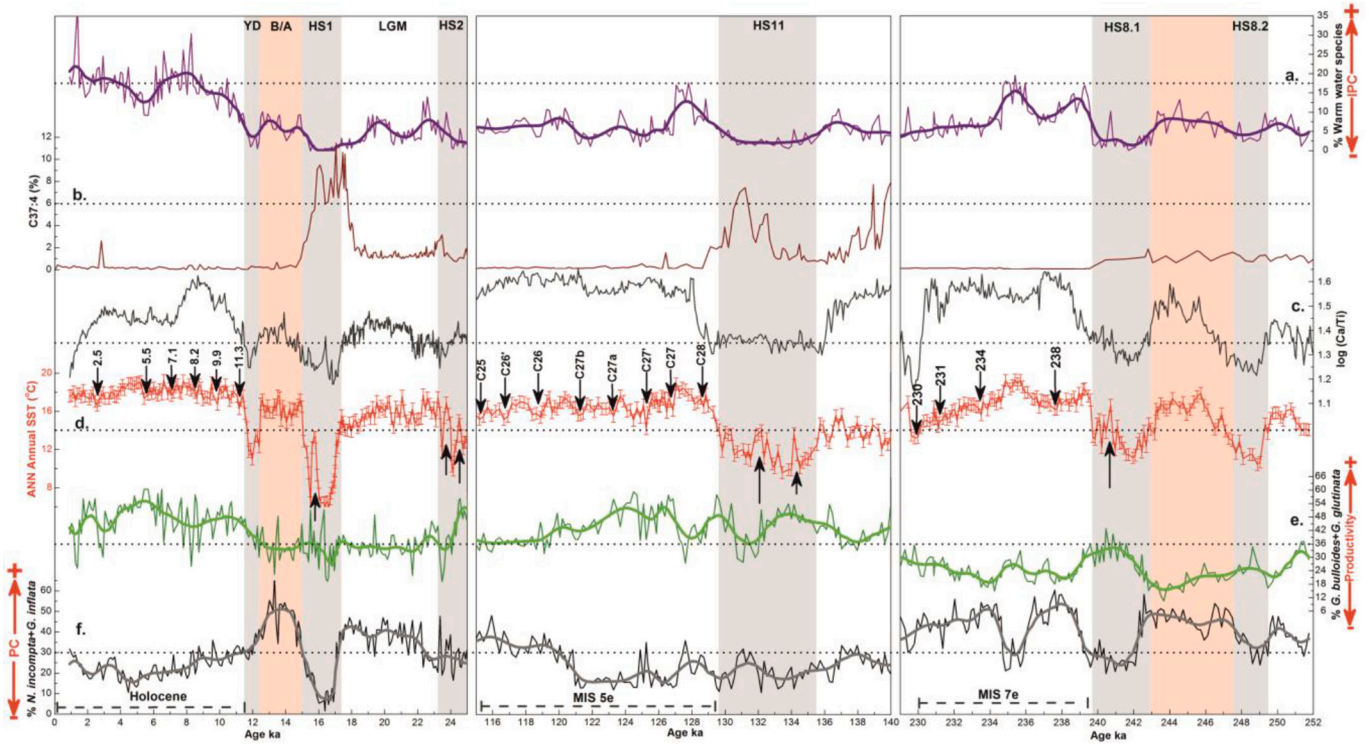

Fig. 3. Comparison of relative abundances of various planktic foraminiferal assemblages with ANN-based annual SST (this study) and log (Ca/Ti) records (Hodell et al., 2015) of IODP Site U1385: (a) % warm water species (*G. ruber*, *T. sacculifer* plexus, *G. siphonifera*, *G. rubescens*, *G. falconensis*, *O. universa* and *P. obliquiloculata*), (b) % C37:4 from core MD01–2444 (Martrat et al., 2007), (c) log (Ca/Ti), (d) ANN-based annual SST (°C), (e) % *G. glutinata* + *G. bulloides* and (f) % *G. inflata* + *N. incompta*. Bold curve shows the FFT smoothening. Vertical grey bars mark the stadials: YD, HS1, HS2, HS11, HS8.2 and HS8.1 whereas the pink bars mark the interstadials: B/A & TIII interstadial. Downward pointing arrows denote the brief cold stadials interrupting the interglacials (Holocene, MIS 5e and 7e). Upward pointing arrows denote the brief warm events interrupting HS1, HS2, HS11 and HS8.1. Horizontal dotted lines are added for visual aid only. (For interpretation of the references to colour in this figure legend, the reader is referred to the web version of this article.)

greatest range in annual SST is observed across TI with temperatures varying from a minimum of ~5.8 °C during HS1 to ~19.3 °C during the Holocene (~6.6 ka). During TII, annual SST values dropped to ~10 °C during HS11 and subsequently increased to ~19.3 °C during MIS 5e (~127 ka, Fig. 3, Table 1). Annual SST across TIII varied from a minimum of ~10.3 °C during HS8.2 to ~19.1 °C during MIS 7e (~235.5 ka). For the terminal stadials (HS1 and HS8.1), the annual SST record shows a complex profile with two sharp drops in SST values separated by a brief rise of ~5–6 °C. The SST profile during HS2 and HS11 seems to be more complex with three phases of SST drops interrupted by two brief intervening SST peaks (Fig. 3). The steepest SST gradient of ~2.1 °C/kyr corresponds to the TI interval, followed by TII with a SST gradient of ~1.5 °C/kyr and TIII with a very low SST gradient of ~0.8 °C/kyr (Fig. 3, Table 1). The estimated average annual SST values during the interglacials are 18.0 °C, 17.0 °C and 16.4 °C for the Holocene, MIS 5e and 7e respectively, which suggests that temperatures during these periods were slightly colder than present (18 °C, Locarnini et al., 2010). Although the SST record suggests relatively stable interglacials, we do register multiple brief episodes of SST fluctuations with amplitudes of ~1.3–3 °C. Several brief cold events interrupted the Holocene at ~11.3, 9.9, 8.2, 7.1, 5.5, 2.5 ka, and MIS 5e at ~128.7, 126.7, 125.5, 123.5, 121.5, 119, 117, and 115.5 ka. Similar cold events appear to have been less frequent during MIS 7e occurring at ~238, 234, 231, and 230 ka (Fig. 3). Our estimated average seasonal SST difference (summer SST-winter SST) for the entire study interval is ~4.8 °C, which is very close to the present day value (5 °C) at the study site (Locarnini et al., 2010). This difference increases during the interstadials and interglacials, while during the stadials it decreases to minimum values (Fig. 4).

5. Discussion

5.1. Climate-induced surface ocean variability along the Iberian Margin during the last three terminations

5.1.1. SST variation

The ANN-based SST record parallels the long-term changes in the $\delta^{18}O$ time series of the Greenland ice core (North Greenland Ice Core Project members, 2004) and the synthetic Greenland record (Barker et al., 2011) across the last three terminations, reflecting the typical Northern Hemisphere pattern of temperature variations along the Iberian Margin (Fig. 5). Comparison of these terminations with respect to SST variations reveals that the sequence of climatic events during TIII is similar to that of TI, despite different orbital configurations. TI was interrupted by one warm and two cold climatic events: HS1, B/A and YD, a sequence identical to the events: HS8.2, an interstadial and HS8.1, overprinting TIII (Fig. 5). The stalagmite records from China also depict the similarity in TIII and TI (Cheng et al., 2009; Duan et al., 2022). However, in terms of duration and SST gradient TI and TIII were characteristically distinct. TI lasted for ~6 kyr with a steep SST gradient of ~2.1 °C/kyr, whereas, TIII spanned ~10 kyr with a gentle SST gradient of ~0.8 °C/kyr (Table 1). This dissimilarity is probably due to different orbital configurations and atmospheric greenhouse gas concentrations (Fig. 5).

Unlike TI and TIII, the sequence of climatic events for TII was unique, as it was interrupted by a single extended stadial HS11 with coldest annual SST of ~10 °C (Table 1). Speleothem records from southern Europe also reveal a climatic event associated with HS11 (Drysdale et al., 2005; Perez-Mejías et al., 2017; Stoll et al., 2022). TII was nearly identical to TI in terms of duration (~6 kyr) and SST gradient (~1.5 °C/

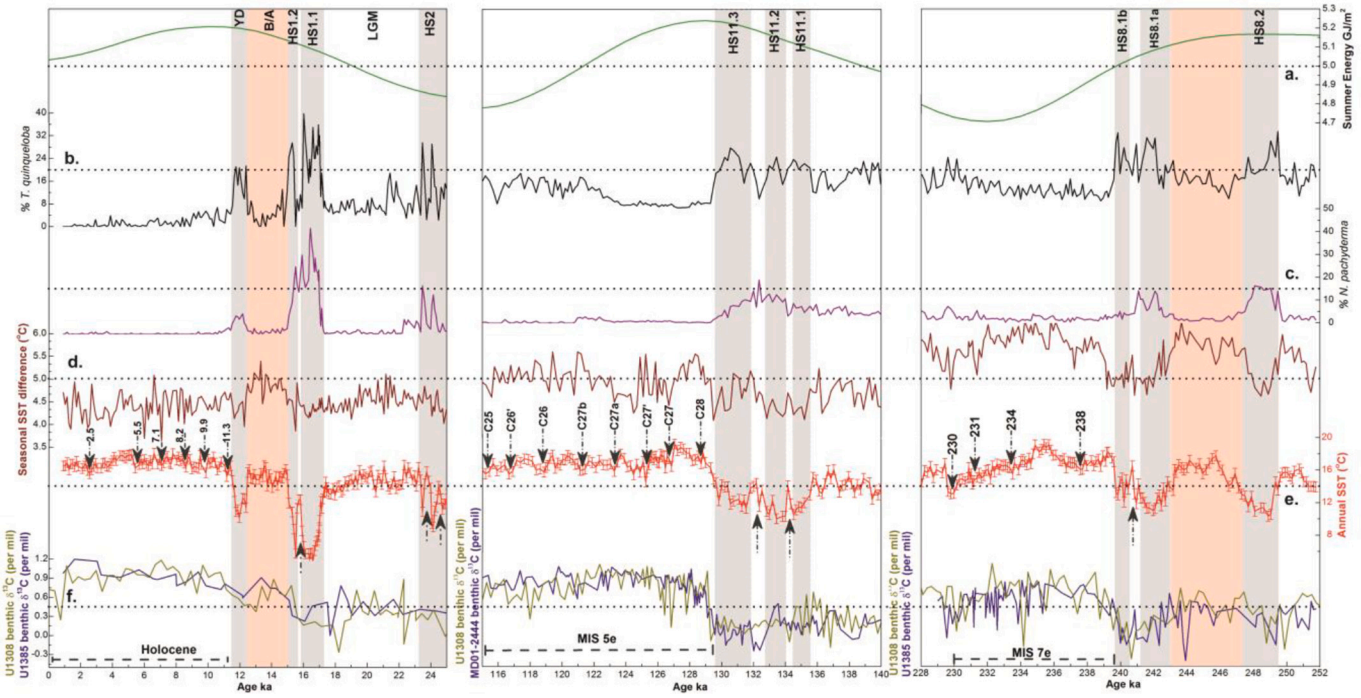

Fig. 4. Comparison between records of IODP Site U1385, integrated summer energy at 65°N and benthic $\delta^{13}C$ records from North Atlantic Ocean: (a) integrated summer energy at 65°N (>275 W/m^2; Huybers, 2006), (b) % *T. quinqueloba*, (c) % *N. pachyderma*, (d) ANN-based seasonal SST difference (summer-winter, °C), (e) ANN-based annual SST (°C) and (f) benthic $\delta^{13}C$ records of sites U1385, MD01–2444 (Iberian margin, Hodell et al., 2023; Tzedakis et al., 2018) and U1308 (North Atlantic IRD belt, Hodell et al., 2008). Vertical grey bars mark the stadials (and its phases): YD, HS1 (HS1.1 & HS1.2), HS2, HS11 (HS11.1, HS11.2 & HS11.3), HS8.1 (HS8.1a & HS8.1b) and HS8.2 whereas the pink bars mark the interstadials: B/A & TIII interstadial. Downward pointing arrows denote the brief cold stadials interrupting the interglacials (Holocene, MIS 5e and 7e). Upward pointing arrows denote the brief warm events interrupting HS1, HS2, HS11 and HS8.1. Horizontal dotted lines are added for visual aid only. (For interpretation of the references to colour in this figure legend, the reader is referred to the web version of this article.)

kyr). This resemblance can be explained by the similarity in orbital configurations and atmospheric greenhouse gas concentrations prevailing during the two terminations (Fig. 5). Another factor that could influence the SST gradient is the extent of continental ice sheets during the periods preceding those terminations (MIS 8, MIS 6 and MIS 2). The elemental records from the Bay of Biscay suggest that continental ice-sheets in NW Europe during MIS 8 were significantly smaller than during MIS 6 and MIS 2 (Toucanne et al., 2009). Thus, the melting of smaller ice sheets over a longer duration (~10 kyr) points towards a relatively weak nature of the MIS 8–7 transition leading to limited changes in ice volume and SST compared with the last two terminations (Lang and Wolff, 2011; Shakun et al., 2015).

Initiation of TI and TIII was marked by stadials featuring a significant decrease in SST from ~15.6 to ~5.8 °C during HS1 and from ~15.1 to ~10.3 °C during HS8.2 (Table 1). Both stadials lasted for about 2 kyr. We also document an intervening warm phase of ~6 °C SST increase during HS1, while a similar warming episode within HS8.2 was largely elusive from the SST record (Fig. 4). Thus, HS1 and HS8.2 were quite different. The complex structure of HS1 was reported from the IODP Site U1308 located in the eastern section of the North Atlantic IRD belt as well (Hodell et al., 2017). Hodell et al. (2017) considered the two cold phases of HS1 as two separate events and referred to them as HS1.1 and HS1.2. Studies from the mid-latitude North Atlantic Ocean (IODP Site U1313, Naafs et al., 2013), Gulf of Cadiz (Voelker et al., 2006) and the Alboran Sea (ODP Site 976, Martrat et al., 2014; Jiménez-Amat and Zahn, 2015) have also recorded a similar SST pattern for the HS1 (Supplementary Fig. S4). Additional evidences for the internal structure of HS1 can be seen from the paleo-precipitation records of tropical and subtropical regions reflecting two distinct hydrologic events that are mechanistically linked to changes in the AMOC strength (e.g. Zhang et al., 2014; Stríkis et al., 2015).

We observe major shifts in certain planktic foraminiferal species abundances corresponding to the SST variation associated with these climatic events. A significant rise in % *N. pachyderma* (a polar species) and *T. quinqueloba* (a sub-polar species) during HS1.1 followed by the predominance of the latter species during HS1.2 suggest a northward propagation of the polar front during HS1.2 (Fig. 4). Both *N. pachyderma* and *T. quinqueloba* were replaced by *N. incompta*, *G. bulloides* and *G. inflata* abundances during the brief warm event. Earlier foraminiferal assemblage based studies from the Iberian Margin have shown a similar pattern of shift in these planktic species abundances (e.g. Lebreiro et al., 1996; Cayre et al., 1999; de Abreu et al., 2003). The climate simulation studies also suggest the northward shift of the thermal front during HS1.2 (e.g. Ziemen et al., 2019). The shift of the thermal front might have affected the regional hydrology in the north-west and south-west Iberian region. Previous studies have revealed coldest/driest conditions with minimal temperate tree expansion in the adjacent landmasses during HS1.1 and a gradual recovery of the tree taxa during HS1.2 (Naughton et al., 2009, 2015; Cutmore et al., 2021).

HS1 was followed by the B/A interstadial, featuring a rapid rise in SST values from ~6.5 °C to ~17 °C within a short span of 0.5 kyr. On the contrary, transitions to warmer conditions during the TIII were more gradual and lasted twice the duration of B/A, even though the prevailing temperatures were similar (~17 °C, Table 1). Moreover, the patterns of SST variation during both interstadials show a brief period of ~2 °C SST drop within its progression (Fig. 4). This climatic cooling episode also had imprints in the European continental records with a coeval decline in the temperate tree taxa implying slightly colder/drier land conditions (Cutmore et al., 2021). B/A was followed by the YD with a rapid drop in SST (of 6 °C) from ~17 to ~11 °C (Fig. 4). This indicates that the climatic cooling was relatively milder as compared to HS1, when the SST values dropped by ~9.8 °C. A simultaneous expansion of steppe taxa and the Mediterranean vegetation as evidenced from sediment cores in the vicinity of the examined site (SU81–18, MD01–2444 and SHAK06-5K)

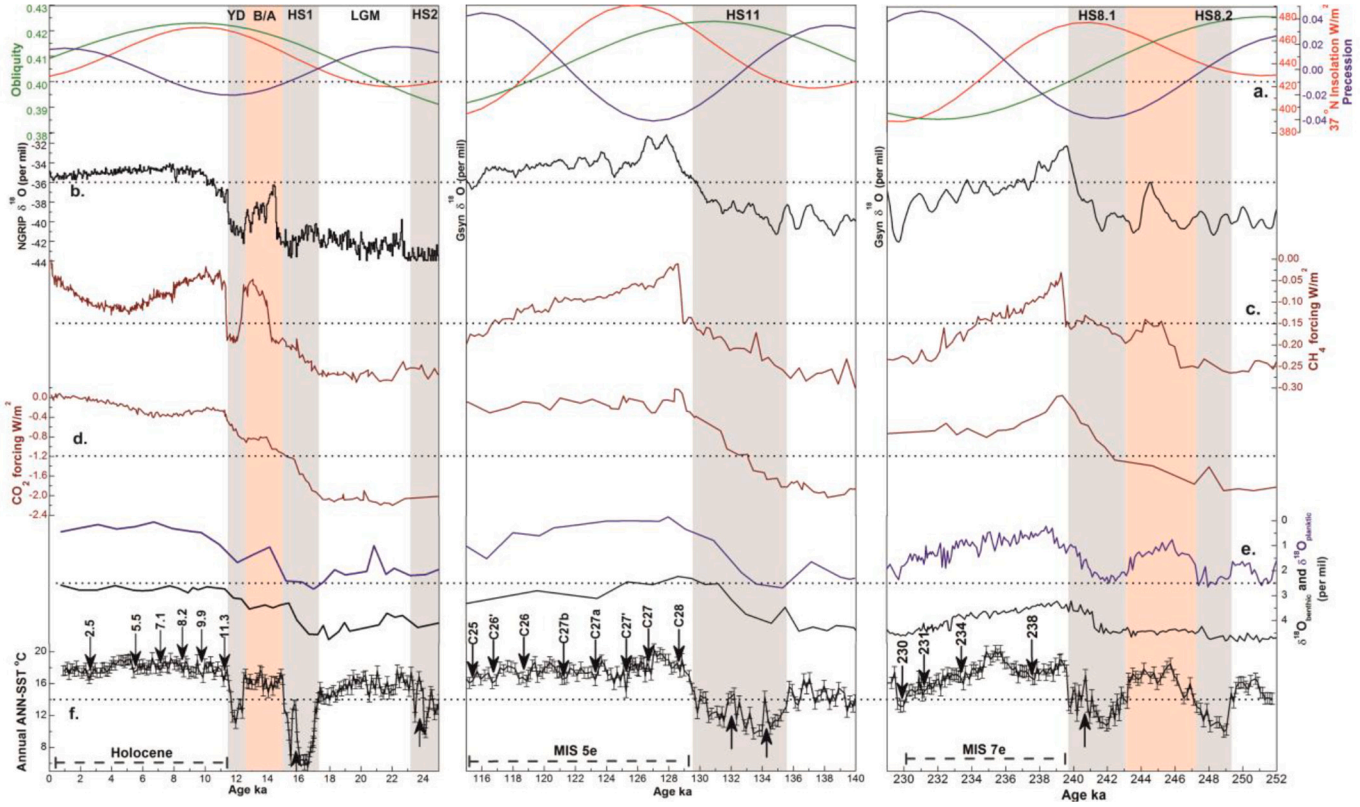

Fig. 5. Comparison between ANN-based annual SST, benthic (*C. wuellerstorfi*) and planktic (*G. bulloides*) oxygen isotope records of IODP Site U1385 with orbital configurations, atmospheric greenhouse gas forcings and oxygen isotope records of Greenland ice cores: (a) 37°N Insolation (W/m^2), Obliquity and Precession (Laskar et al., 2011) (b) NGRIP (North Greenland Ice Core Project members, 2004) and Greenland synthetic δ^{18}O (Barker et al., 2011) records (per mil), (c) CH_4 forcing (W/m^2, Köhler et al., 2017), (d) CO_2 forcing (W/m^2, Köhler et al., 2017), (e) benthic and planktic δ^{18}O (per mil) records (Hodell et al., 2015; Hodell et al., 2023) and (f) ANN-based annual SST (°C). Vertical grey bars mark the stadials: YD, HS1, HS2, HS11, HS8.2 and HS8.1 whereas the pink bars mark the interstadials: B/A & TIII interstadial. Downward pointing arrows denote the brief cold stadials interrupting the interglacials (Holocene, MIS 5e and 7e). Upward pointing arrows denote the brief warm events interrupting HS1, HS2, HS11 and HS8.1. Horizontal dotted lines are added for visual aid only. (For interpretation of the references to colour in this figure legend, the reader is referred to the web version of this article.)

attest to a moderate climatic cooling (Turon et al., 2003; Tzedakis et al., 2018; Cutmore et al., 2021). A climatic transition from an interstadial to HS8.1 during TIII, was also present during the TI transitioning from the B/A to the YD with a drop in SST values from ~17 °C to ~11 °C (Table 1). However, the SST variation pattern of HS8.1 was nearly identical to HS1 with two cold phases sandwiching a brief warm event with an amplitude of ~5 °C, although HS8.1 was slightly warmer and lasted a little longer than HS1 (Fig. 4).

The structure of HS11 (equivalent of the TII stadial event) was relatively more complex consisting of three cold phases (HS11.1, HS11.2 & HS11.3) and two warm phases. Our SST record reveals HS11.2 as the coldest phase within the HS11 complex, followed by HS11.1 and HS11.3 phases (Fig. 4). The cold phases HS11.1 and HS11.2 sandwich a brief warm event with SST rise of ~3 °C, while the other warm event between HS11.2 and HS11.3 was relatively warmer (~4 °C) than the preceding one. This three-phase cooling structure of HS11 is also supported by *T. quinqueloba* abundance maxima. Significant decrease in *T. quinqueloba* abundance corresponds to the two warm phases (Fig. 4). A similar structure of HS11 can also be noticed in alkenone and Mg/Ca based SST records of core MD01–2444, (Tzedakis et al., 2018, SW Iberian Margin) and the Alboran Sea SST records (Supplementary Fig. S4, Martrat et al., 2014; Jiménez-Amat and Zahn, 2015). A recently published *G. bulloides* δ^{18}O record from the Gulf of Cadiz also shows identical variations in line with the above mentioned records during the HS11 complex (Sierro et al., 2020). The pollen records of core MD01–2444 showing prominent fluctuations in concert with the SST variations suggest that the climatic events within the HS11 complex left their imprints in European continental records (Drysdale et al., 2004, 2005; Allen and Huntley, 2009; Moseley et al., 2015; Regattieri et al., 2017; Tzedakis et al., 2018).

Each of the last three terminations display unique features with regard to millennial events. TI and TIII were each interrupted by multiple climatic events, whereas TII was interrupted by a single extended climatic event. The stadials interrupting TIII (HS8.2 and HS8.1) and TI (HS1 and YD) differ in terms of timing, duration and SST. HS8.2 and HS8.1 might be considered equivalent to HS2 and HS1 (Perez-Mejías et al., 2017). Integration of our SST record with the benthic δ^{13}C records of IODP sites U1308 and U1385 supports the analogy between HS8.2 and HS8.1 with HS2 and HS1 (Fig. 4). Low benthic δ^{13}C values during TIII indicate reduced ventilation of deep-water similar to HS2 and HS1 (Obrochta et al., 2014). All four events (HS8.2, HS8.1, HS2 and HS1) are associated with IRD peaks in the North Atlantic Ocean (Channell and Hodell, 2013; Obrochta et al., 2014), whereas IRD deposition is considerably weaker in the IRD belt during the YD. Although HS8.2 and HS2 appear similar, HS2 is followed by the last glacial maxima (e.g. Clark et al., 2004; Hall et al., 2006), whereas the glacial maxima of MIS 8 occurred before HS8.2 (Hughes and Gibbard, 2018). Alternatively, HS8.2 may be considered to be a part of TIII, which is supported by the stalagmite records from Austria (Wendt et al., 2021) and China (Cheng et al., 2009; Duan et al., 2022).

5.1.2. Role of the European Ice-sheet Complexes in shaping the anatomy of the recorded Heinrich stadials: a possible mechanism

Previous studies from the Iberian Margin present the classic Heinrich

stadial view of AMOC weakening due to freshwater release into the high-latitude North Atlantic, which in turn caused severe cooling episodes at the mid-latitudes (e.g. Cayre et al., 1999; Martrat et al., 2007; Voelker et al., 2009; Rodrigues et al., 2011; Martin-Garcia et al., 2015). However, increasingly detailed proxy-based reconstructions and model simulation studies of the Heinrich stadial and the associated climate-ocean perturbations have revealed a more complex structure (with multiple phases) than previously described (e.g. Naafs et al., 2013; Tzedakis et al., 2018; Ziemen et al., 2019). Our SST records for the stadials HS1, HS2, HS11 and HS8.1 reveal intervening brief warm phases, presenting a 'W' shaped pattern of the SST record, which was first coined by Martrat et al. (2014) (Fig. 4). We also document summertime warming (seasonal SST difference) coeval with the brief warm event within HS1, HS2, HS11 & HS8.1 (Fig. 4). It is believed that HS1 was not triggered by the melting of Laurentide ice-sheets, instead increased freshwater forcing from the melting of the EISC may have weakened the AMOC initially (Peck et al., 2006; Toucanne et al., 2010, 2015; Henry et al., 2016) owing to its close proximity to the deep water convection sites (Roche et al., 2010). Subsequent changes in the low to mid-latitude atmospheric water cycle (Landais et al., 2018) caused summertime warming in northern Europe (Boswell et al., 2019) to promote further melting of the EISC. Enhanced melt water discharge from the EISC weakened the AMOC considerably (Skinner and Shackleton, 2006; Bohm et al., 2015) and subsequently led to the warming in the intermediate depth waters (e.g. Shaffer et al., 2004; Marcott et al., 2011; Ezat et al., 2014). The intermediate depth warming may have played a pivotal role in triggering the collapse of the marine-based ice-sheets including the Hudson Strait, thus forcing the Laurentide ice-sheet melting to play the dominant role during HS1.2 (Hodell et al., 2017; Max et al., 2022).

Similar changes might have also occurred during HS2, HS11 and HS8.1, thus contributing to cause the characteristic 'W' pattern of the SST record (Fig. 4). Since the EISC was larger in extent during the Penultimate Glacial Maximum as compared to the Last Glacial Maximum (Ehlers et al., 2011; Ivanovic et al., 2018), the increased melting episodes may have caused a more peculiar SST pattern for HS11.

5.1.3. Paleoproductivity and sea-surface circulation

The record of past changes in surface hydrography off the Iberian Margin provides crucial insights into the dynamics of the regional atmospheric circulation patterns in response to the rapid climatic oscillations during deglaciations (e.g. Incarbona et al., 2010; Ausín et al., 2020). We used planktic foraminiferal proxies to reconstruct the productivity and sea-surface circulation during the last three terminations. Our productivity proxy record (*G. bulloides* + *G. glutinata*) reveals a pattern of variation opposite to the SST changes. The surface productivity during the cold phases of HS1 (HS1.1 and HS1.2) was in general low, although it increased abruptly as the temperature reached to its minimum. Comparatively the productivity during HS1.1 was slightly higher than during HS1.2. The northward shift of the polar front during HS1.2 may be a factor responsible for the increase in productivity (Fig. 3). The northward shift of the polar front resulted in the reduction of freshwater supply associated with the melting of drifting icebergs, consequently the surface stratification weakened in the study region (Lebreiro et al., 1997; Eynaud et al., 2000; Thomson et al., 2000). This favoured the wind-induced mixing which might have led to the productivity increase during HS1.2. A similar pattern of primary productivity variation during HS1 has also been documented in coccolithophore records from core SHAK06-5K (Ausín et al., 2020).

The two productivity minima during HS1 are probably related to the enhanced supply of less saline surface waters to the Iberian Margin due to the melting of drifting iceberg armadas as evident from alkenone C37:4 (%) records of core MD01–2444 (Fig. 3, Martrat et al., 2007), which caused strong surface water stratification and reduction of the upwelling induced productivity (Voelker et al., 2009; Incarbona et al., 2010; Salgueiro et al., 2010). The rapid rise in productivity condition corresponding to the temperature minima during the cold phases of HS1 can be explained by the increased influence of westerly winds over the Iberian Peninsula due to the southward migration of the North Atlantic jet stream forced by a southward shift of the polar front (Costas et al., 2016; Wolf et al., 2018, 2019). The increased influence of westerlies might have resulted in the vertical mixing of the surface waters, thus causing a productivity increase during the cold phases of HS1. It is also possible that the turbulent mixing from the drifting of melting icebergs caused nutrient advection to the surface and thereby an increase in productivity during the cold phases of HS1 (Lebreiro et al., 1997; Eynaud et al., 2000; Thomson et al., 2000). The productivity proxy record reveals a similar pattern of variation for the stadials YD, HS2, HS11 and HS8.2 as documented for HS1 (Fig. 3, Table 2). This reflects a general pattern of low productivity conditions for the stadials with an abrupt increase during the temperature minima. However HS8.1 shows an overall productivity increase, which could be due to the increased vertical mixing of the less stratified surface waters off the Iberian Margin (Fig. 3).

Present day surface hydrography of the study area is modulated by the seasonal migration of the Azores High and the two main surface currents, PC and IPC (Peliz et al., 2005). Thus, it becomes imperative to study the past variations in the PC and IPC influences, as these currents play a crucial role in modulating the surface productivity in this region. Previous studies have shown that the AF was displaced southward during HS1, while it was in a northern position during the B/A due to the AMOC weakening and strengthening, respectively (Schwab et al., 2012; Repschläger et al., 2015). The faunal proxy record reveals that during the interstadial warming, particularly the B/A event of TI and the interstadial event of TIII, the overall productivity was low (Fig. 3). Increased abundances of warm water species and > 15 °C SST values suggest the prevalence of warm subtropical waters. Since the AF was displaced north during B/A, the study area was dominated by warm and oligotrophic waters of the IPC, thereby resulting in the productivity decrease. It is also possible that the expansion of the subtropical gyre during B/A resulted in the enhanced influence of nutrient-depleted warm waters (Reißig et al., 2019). Earlier studies from the study area have also reported decreased productivity during the B/A (Schwab et al., 2012; Palumbo et al., 2013; Nave et al., 2018). However, coccolithophore records from core SHAK06-5K show an increase in productivity during this period (Incarbona et al., 2010; Ausín et al., 2020; Argenio et al., 2021). This inconsistency could be due to the differential seasonal response of the two plankton groups. *G. bulloides* and *G. glutinata* proliferate during summer upwelling conditions (Salgueiro et al., 2008), whereas coccolithophores prefer more stratified winter/spring conditions along the Iberian Margin (Abrantes and Moita, 1999; Abrantes et al., 2009). It is also possible that coccolithophores proliferated during the B/A period due to nutrients brought by riverine discharge owing to the increase in winter precipitation (e.g. Moreno et al., 2010; Naughton et al., 2015).

The deglacial climate variability has also significantly influenced the PC, the south-westward flowing branch of the NAC (e.g. Palumbo et al., 2018). Planktic foraminiferal proxies indicating the influence of the PC (*N. incompta* + *G. inflata*) suggest its general weakening during the stadials and intensification during the interstadials (Table 2). However, there has been a slight increase in abundances of these species during the intervening brief warm events of the stadials HS1, HS2, HS11 and HS8.2 indicating some influence of the PC (Fig. 3). Hence the PC/NAC was not completely shut down during the Heinrich or Heinrich-type stadials which agrees with the previous results suggesting only a slowdown of the heat transfer from the tropics to the poles during the stadials (e.g. McManus et al., 2004; Repschläger et al., 2021). Intriguingly, our records show a slightly lagged response of the PC to SST variation during HS8.1, but not for the other stadials (Fig. 3).

Table 2
A summary of the inferred migration of polar/subpolar front, productivity change and the dominant wind regime with PC and IPC influence for the events documented at IODP Site U1385.

Interval	Event	Age range (ka)	Polar/subpolar front migration	Relative change in productivity	PC influence	IPC influence	Dominant wind regime
	HS2	25–23.2	Migrated south towards IbM	Overall low to moderate productivity with brief peaks	Decreased	Decreased	Westerly winds
	HS1	17.2–15	Migrated south towards IbM	Overall low productivity with brief peaks	Decreased	Decreased	Westerly winds
Termination I	B/A	15–12.5	Migrated north away from IbM	Overall low productivity with brief peaks	Increased	Increased	Trade winds
	YD	12.5–11.6	Migrated south towards IbM	Low productivity	Decreased	Decreased	Westerly winds
Termination II	HS11	135.5–129.5	Migrated south towards IbM	Overall low to moderate productivity with brief peaks	Decreased	Decreased	Westerly winds
	HS8.2	249.5–247.5	Migrated south towards IbM	Overall low productivity with brief peaks	Decreased	Decreased	Westerly winds
Termination III	Interstadial	247.5–243	Migrated north away from IbM	Overall low productivity with brief peaks	Increased	Increased	Trade winds
	HS8.1	243–239.5	Migrated south towards IbM	Overall low productivity with an increasing trend	Decreased	Decreased	Westerly winds
	Early	11.6–8		Overall moderate productivity with brief peaks	Increased	Increased	
Holocene	Middle	8–5		Overall high productivity with brief drops	Decreased	Decreased	
	Late	5–1		Overall high productivity with a decreasing trend	Increased	Increased	
	Early	129.5–127		Overall moderate productivity with brief peaks	Increased	Increased	
MIS 5e	Middle	127–120.5		Overall high productivity with brief drops	Decreased	Decreased	Trade winds
	Late	120.5–115		Overall moderate productivity with a decreasing trend	Increased	Increased	
	Early	239.5–236.5		Overall low productivity with brief peaks	Increased	Increased	
MIS 7e	Middle	236.5–234		Overall low productivity with slight productivity increase	Decreased	Decreased	
	Late	234–230.5		Overall low productivity with an increasing trend	Increased		

5.2. Ocean-climate variability during the interglacials: Holocene, MIS 5e and 7e

5.2.1. SST variation on longer to short time scales

Long-term trends in the SST record show a broad similarity in the climatic progression of the three interglacials despite the differences in the orbital configurations and atmospheric greenhouse gas concentrations (Fig. 5). A rapid SST rise of ~6–7 °C during the onset of these interglacials seems to be a common feature. Following the interglacial onset, SST values increased to a maximum for a brief period. Thereafter, a slight cooling of ~2–4 °C was recorded during the middle part of the interglacials. This cooling episode was followed by a brief period of warming reaching to the second SST maximum, and then switching over to a cooling phase in the later part of the interglacials (Fig. 5, Table 1). The late stage cooling of the interglacials is evident in the abundance record of *T. quinqueloba* (Fig. 4). Our findings gain support from the pollen records from Europe showing synchronous changes in temperate and Mediterranean tree taxa with their expansion during the warmer and reduction during the colder conditions (Sanchez-Goñi et al., 1999; Tzedakis, 2003; Tzedakis et al., 2018; Naughton et al., 2007; Roucoux et al., 2008; Sadori et al., 2016; Oliveira et al., 2018; Cutmore et al., 2021).

We notice six distinct short-term cooling events of ~1.3–2 °C within the Holocene (Fig. 6). One of the cold events is the '8.2 ka' recording a ~1.5 °C SST drop after attaining temperatures of ~18.8 °C. Pollen records from core SHAK06-5K, corroborate the SST decrease by reflecting a significant decrease in the thermophilous woodland over the adjacent landmasses (Cutmore et al., 2021). Our SST records in conjunction with model results and other climate proxy records reveal a climatic cooling of several centuries between ~8.9 and 8 ka (Rohling and Palike, 2005; Ellison et al., 2006; Morrill et al., 2013). Apart from the 8.2 ka event, five more cold events interrupted the Holocene at ~11.3, 9.9, 7.1, 5.5, and 2.5 ka (Fig. 6). Signatures of these cold episodes have been recorded in both the high (Northern North Atlantic, Bond et al., 1997, 2001; Oppo et al., 2003) and low (Mediterranean Sea, Cacho et al., 1999; Martrat et al., 2014; NW Iberian Margin, Palumbo et al., 2013; and subtropical west Africa, deMenocal et al., 2000) latitudes of the North Atlantic Ocean. Hence, these short-term cold episodes have left their imprints throughout the North Atlantic Ocean and the adjoining regions.

Similar to the Holocene, MIS 5e was also interrupted by several brief cold events at ~128.7, 126.7, 123.5, 121.5, 119, and 115.5 ka with SST decrease of ~2–3 °C (Fig. 6). Counterparts of these cold events were recorded from the sub-polar North Atlantic Ocean (C28, C27, C27a, C27b, C26, C25; Oppo et al., 2006). Regional signatures of these cold events were also detected in the pollen and speleothem records of Europe as cold/dry episodes (Couchoud et al., 2009; Milner et al., 2013; Regattieri et al., 2016; Tzedakis et al., 2018). We record two additional cold events C27' at ~125.5 ka and C26' at 117 ka, which were present in the sediment core MD01–2444 (Fig. 6, Tzedakis et al., 2018), but absent in the sub-polar North Atlantic, indicating a possible regional extent of these stadials.

Unlike the Holocene and MIS 5e, the MIS 7e interglacial seems largely stable in terms of the intra-interglacial variability. Nonetheless, the SST record reveals four brief cold events interrupting the MIS 7e at ~238, 234, 231, and 230 ka (Fig. 6), which can also be observed in the SST record of core MD01–2444/−2443 (Martrat et al., 2007; de Abreu et al., 2005). Paleo-vegetation and precipitation records of SW Europe confirm the presence of cold and dry conditions in the surrounding landmasses during these brief events (Roucoux et al., 2008; Sadori et al., 2016; Pickarski and Litt, 2017; Wendt et al., 2021). Hence, the three interglacials are different from each other in respect of the pattern of intra-interglacial short-term climate variability.

5.2.2. Intra-interglacial variability of Holocene, MIS 5e and 7e interglacials: the AMOC link

A cooling trend from middle to late stages of the interglacials is a

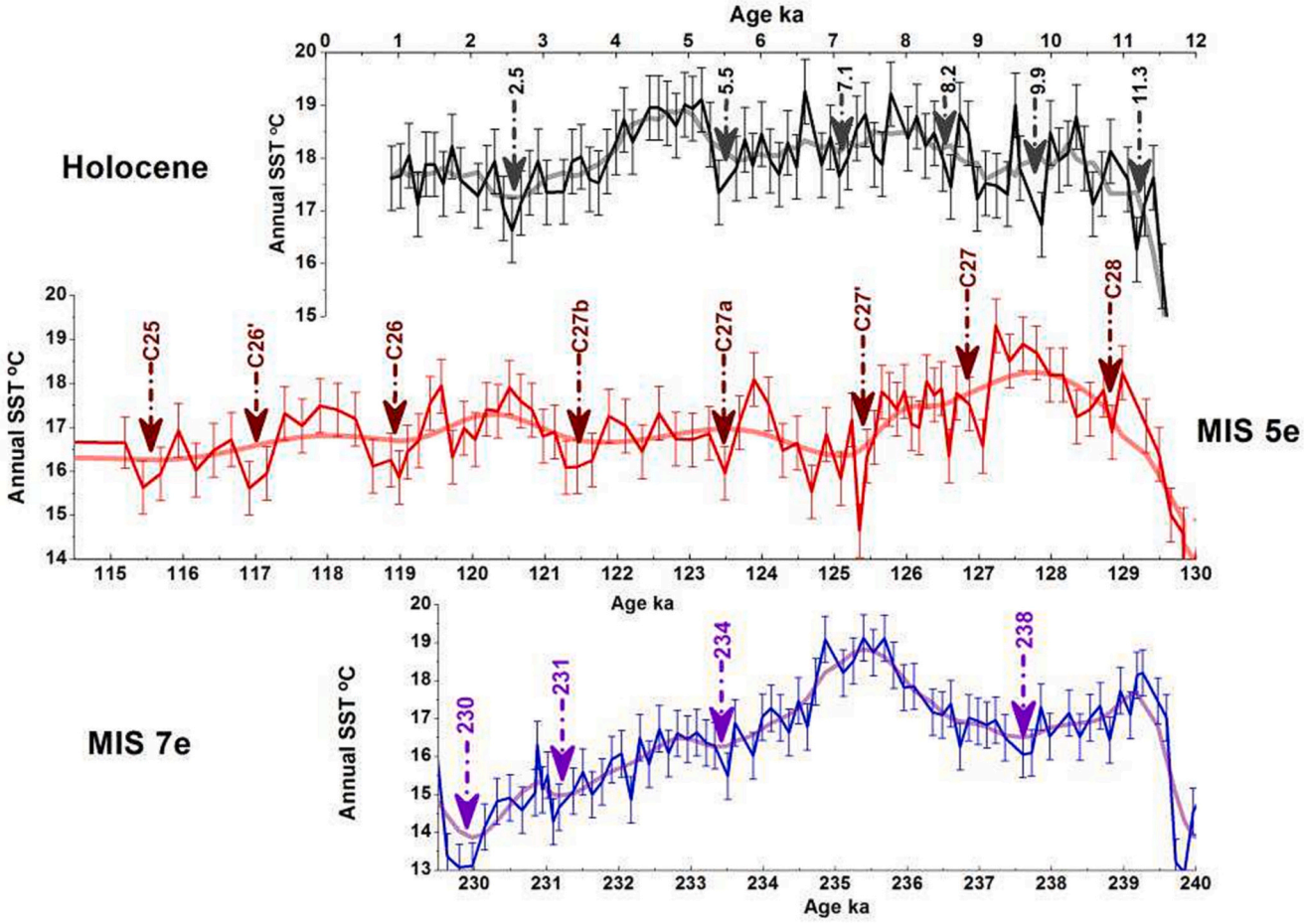

Fig. 6. Comparison of ANN-based annual SST records of the three interglacials (Holocene, MIS 5e & 7e) at IODP Site U1385. Bold curve shows the FFT smoothening. Downward pointing arrows denote the brief cold stadials interrupting the interglacials.

dominant feature of our SST record (Fig. 5, Table 1). The long-term cooling trend of the interglacials was superimposed by multiple centennial-millennial scale climatic events (Fig. 6). However, the timing, duration and frequency of these climatic events varied among these interglacials. Similar to the present study, the cooling trends during MIS 5e and the Holocene have been reported from the Alboran Sea (Martrat et al., 2014; Jiménez-Amat and Zahn, 2015) and the Iberian Margin (Bakker et al., 2014). Benthic $\delta^{13}C$ records from the Eirik Drift reveal several episodes of abrupt changes in the NADW formation for the five most recent interglacials (Galaasen et al., 2020). Another $\delta^{13}C$ record from the IRD belt of the North Atlantic Ocean also show multiple short-term variations during the three interglacials (Fig. 4, Hodell et al., 2008). The short-lived variations in $\delta^{13}C$ benthic record from the study area (U1385, MD01–2444) have been attributed to the changes in deep water circulation (Fig. 4, Hodell et al., 2023; Tzedakis et al., 2018). Therefore, we argue that the brief cold events recorded at Site U1385 are probably related to the reduction in the NADW convection possibly triggered by the enhanced freshwater release into the North Atlantic (Kleiven et al., 2008). This is in line with the previous results documenting a large-scale SST decrease from the Iberian Margin during the Heinrich stadials caused by the freshwater perturbations at high latitudes (e.g. Cayre et al., 1999; de Abreu et al., 2005; Eynaud et al., 2009; Rodrigues et al., 2011). This provides a potential explanation for the low magnitude variability within MIS 7e, as the integrated summer insolation energy was relatively low during MIS 7e (Huybers, 2006), causing only moderate meltwater release and hence only minor variations in deep water convection (Fig. 4).

5.2.3. Sea-surface circulation and productivity changes

The faunal proxy records indicate a general high productivity condition during the interglacials superimposed by the short-term fluctuations owing mainly to the changes in the strength and position of the Azores High along with the influence of the surface current system (PC and IPC, Fig. 3). Early and late parts of the interglacials show increased influence of PC and IPC attributing low productivity conditions. Conversely, the influence of PC and IPC during the middle parts was relatively reduced leading to the increase of biological productivity. However, the productivity increase during the middle part of MIS 7e was relatively moderate (Fig. 3, Table 2). Patterns of variation of the productivity proxy record show an in general inverse relationship to the IPC associated warm water assemblage and the PC associated assemblage (Fig. 3). This suggests that upwelling induced productivity changes during the interglacials are primarily influenced by the fluctuations in the Azores High strength and its meridional migration, similar to the modern conditions where the seasonal wind-induced upwelling/vertical-mixing modulates the surface productivity in the SW Iberian Margin. Strengthening and northward shift of the Azores High led to the increased influence of the north-easterly trade winds to the study region, thereby contributing to the productivity increase. In contrast, weakening and southward shift of the Azores High resulted in the strengthening of the south-westerly winds that inhibited the coastal upwelling (e.g. Salgueiro et al., 2014; Singh et al., 2015; Palumbo et al., 2013, 2018; Martins et al., 2018; Argenio et al., 2021). However, this was not always the case, for instance during the brief period between 236 and 234 ka, when warm water species and productivity proxy both show an increase (Fig. 3), indicating increased influence of the IPC at the study

site. It is also possible that the enhanced mixing of the surface waters caused the advection of nutrient-laden subsurface waters to the surface and thus causing the productivity increase (Fig. 3). Our explanation gains support from the simultaneous increase in the abundance of *G. glutinata* that flourishes in the well-mixed surface waters off the Iberian Margin (Fig. 2, Vautravers and Shackleton, 2006; Singh et al., 2015).

Another exception to this interglacial pattern is the IPC variation during the MIS 7e showing a two-fold fluctuation in its influence. In general, a strong IPC influence was evident during the first half of MIS 7e, which weakened considerably during the second half (Fig. 3). Superimposed on the long-term interglacial pattern, the surface ocean conditions further show prominent short-scale fluctuations at centennial to sub-centennial timescale. During the brief cold events of the interglacials, we observe a productivity increase in concert with the reduced influence of PC and IPC (Fig. 3). Our findings are corroborated by a recent study from the core SHAK06-5K demonstrating productivity peaks corresponding to the brief cold events interrupting the Holocene (Ausín et al., 2020).

The faunal productivity records of Site U1385 reveal a general pattern of low productivity during the stadials and interstadials and high productivity during the interglacials. This pattern suggests a common large-scale mechanism at play here, which is in agreement with earlier studies from this region (Incarbona et al., 2010; Salgueiro et al., 2010). Reductions in AMOC during the stadials resulted in Northern Hemisphere cooling and an associated southward migration of the atmospheric and hydrographic frontal systems (Barker et al., 2009; Repschläger et al., 2015). Subsequently, freshwaters from melting icebergs reached the Iberian Margin and inhibited upwelling to cause a decline in productivity. Meanwhile during the interglacials, AMOC strengthening resulted in the northward migration of the atmospheric and hydrographic frontal systems (Barker et al., 2009; Repschläger et al., 2015). This probably caused the increased influence of trade winds over the study region, thereby promoting productivity increase. Low productivity during the interstadials and early parts of the interglacials was probably due to the expansion of the subtropical gyre (Reißig et al., 2019), resulting in the enhanced influence of warm and nutrient-depleted waters of the subtropical gyre in the study area.

6. Conclusions

Planktic foraminiferal assemblage and SST data from IODP Site U1385 provided a centennial-millennial scale record of surface ocean conditions off SW Iberia for the last three terminations (TI, TII & TIII) and the subsequent interglacials (Holocene, MIS 5e & 7e). The last two terminations (TI & TII) show similar characteristics in terms of duration (~6 kyr) and SST gradient (~1.5 to 2.1 °C/kyr), meanwhile TIII shows a longer duration (~10 kyr) with a gentle SST gradient (~0.8 °C/kyr). While this would seem to indicate a close correlation between the climatic events interrupting TI and TII, instead our records suggest that TI was interrupted by HS1, B/A & YD, a sequence identical to HS8.2, an interstadial & HS8.1 during TIII whereas TII was interrupted by a single extended event, HS11. Moreover, HS8.2 and HS8.1 resemble HS2 and HS1 in timing, thereby indicating the uniqueness of the last three terminations. The stadials (HS1, HS2, HS11 & HS8.1) portray a complex history with two or three cold phases separated by (a) brief warm event (s). Initial cold phase(s) of the stadials were probably influenced by the EISC melting whereas the Laurentide Ice-sheet melting probably influenced the latter cold phase, with the mid-latitude summertime warming and intermediate-depth water mass warming possibly playing a connecting role between these cold phases. Our records also reveal prominent changes in surface productivity and surface currents (PC & IPC) during the last three terminations. An overall low productivity condition superimposed by brief productivity peaks were recorded during these terminations with decreased (increased) influence of the surface currents during the stadials (interstadials). The interglacials, Holocene, MIS 5e and 7e, showed broad similarities in their climatic progression with steep SST rise of ~6–7 °C during the interglacial onsets. The early part of the interglacials showed increase in SST and surface currents causing low productivity conditions whereas the middle part showed relatively reduced SST and surface water conditions with high productivity. The late part of the interglacials showed SST and productivity decline with increased influence of the surface currents. An exception to this general interglacial pattern was the IPC during MIS 7e, showing a twofold variation with increase and decrease in its influence during the first and second half of MIS 7e respectively. The long-term SST trend of interglacials was superimposed by multiple brief cold events. Several such events interrupted the Holocene (~11.3, 9.9, 8.2, 7.1, 5.5, 2.5 ka) and MIS 5e (C28, C27, C27', C27a, C27b, C26, C26', C25) whereas only four cold events interrupted the MIS 7e (~238, 234, 231, & 230 ka). These brief oscillations in temperature were probably triggered by freshwater addition due to the melting of Northern Hemisphere ice-sheets and the subsequent reduction of AMOC.

Declaration of Competing Interest

One of the authors is an editorial board member of Global and Planetary Change. The review process was handled by an independent editor and the authors have no other competing interests to declare.

Data availability

Data will be made available on request.

Acknowledgements

We gratefully acknowledge the IODP for providing samples to carry out this study. We thank the shipboard team (scientists, crew members and technical staff on-board R/V JOIDES RESOLUTION) of IODP Expedition 339. We are grateful to M. Kucera and E. Salgueiro for providing the MARGO North Atlantic and Iberian margin planktic foraminiferal database respectively. We also thank the two anonymous referees for their constructive comments that helped us to improve the manuscript significantly. HS acknowledges UGC for Senior Research Fellowship (419/(CSIR-UGC NET JUNE 2018)). Financial support from the IODP-India, NCPOR, MoES (NCAOR/IODP/17.7/10), IoE Incentive Grant BHU (Dev. Scheme No. 6031) and DST-SERB (CRG/2021/002212) to ADS is acknowledged. PS thanks the Climate Change Programme of DST (DST/CCP/CoE/80/2017-G) for Junior Research Fellowship. AHLV acknowledges contributions from Portuguese national funds from FCT-Foundation for Science and Technology through projects UIDB/04326/2020, UIDP/04326/2020 and LA/P/0101/2020. DAH was supported by the Natural Environmental Research Council (NERC).

Appendix A. Supplementary data

Supplementary data to this article can be found online at https://doi.org/10.1016/j.gloplacha.2023.104100.

References

Abrantes, F., Moita, M.T., 1999. Water column and recent sediment data on diatoms and coccolithophorids, off Portugal, confirm sediment record of upwelling events. Oceanol. Acta 22, 319–336.

Abrantes, F., Lopes, C., Rodrigues, T., Gil, I., Witt, L., Grimalt, J., Harris, I., 2009. Proxy calibration to instrumental data set: Implications for paleoceanographic reconstructions. Geochem. Geophys. Geosyst. 10 (9), Q09U07.

Allen, J.R.M., Huntley, B., 2009. Last Interglacial palaeovegetation, palaeoenvironments and chronology: a new record from Lago Grande di Monticchio, southern Italy. Quat. Sci. Rev. 28, 1521–1538.

Ambar, I., Serra, N., Brogueira, M.J., Cabecadas, G., Abrantes, F., Freitas, P., Goncalves, C., Gonzalez, N., 2002. Physical, chemical and sedimentological aspects of the Mediterranean outflow off Iberia. Deep-Sea Res. II Top. Stud. Oceanogr. 49, 4163–4177.

Anderson, R.F., Ali, S., Bradtmiller, L.I., Nielsen, S.H.H., Fleisher, M.Q., Anderson, B.E., Burckle, L.H., 2009. Wind-driven upwelling in the Southern Ocean and the deglacial rise in atmospheric CO2. Science 323 (5920), 1443–1448.
Argenio, C., Flores, J.A., Balestra, B., Amore, F.O., 2021. Reconstructing Ocean surface dynamics over the last- 25 kyr at "Shackleton Site" IODP-U1385. Palaeogeogr. Palaeoclimatol. Palaeoecol. 579, 110587.
Ausín, B., Hodell, D.A., Cutmore, A., Eglinton, T.I., 2020. The impact of abrupt deglacial climate variability on productivity and upwelling on the southwestern Iberian margin. Quat. Sci. Rev. 230, 106–139. https://doi.org/10.1016/j.quascirev.2019.106139.
Bakker, P., Stone, E.J., Charbit, S., Gröger, M., Krebs-Kanzow, U., Ritz, S.P., Varma, V., Khon, V., Lunt, D.J., Mikolajewicz, U., Prange, M., 2014. Last Interglacial temperature evolution-A model inter-comparison. Clim. Past 9, 605–619.
Bard, E., Rostek, F., Turon, J.L., Gendreau, S., 2000. Hydrological impact of Heinrich events in the subtropical Northeast Atlantic. Science 289 (5483), 1321–1324.
Barker, S., Knorr, G., 2021. Millennial scale feedbacks determine the shape and rapidity of glacial termination. Nat. Commun. 12, 2273. https://doi.org/10.1038/s41467-021-22388-6.
Barker, S., Diz, P., Vautravers, M.J., Pike, J., Knorr, G., Hall, I.R., Broecker, W.S., 2009. Interhemispheric Atlantic seesaw response during the last deglaciation. Nature 457 (7233), 1097–1102.
Barker, S., Knorr, G., Edwards, R., Parrenin, F., Putnam, A., Skinner, L., Wolff, E., Ziegler, M., 2011. 800,000 years of abrupt climate Variability. Science 334, 347–351.
Bé, A.W.H., Tolderlund, D.S., 1971. Distribution and ecology of living planktonic foraminifera in surface waters of the Atlantic and Indian Oceans. In: Funnel, B.M., Riedel, W.R. (Eds.), The Micropaleontology of Oceans. Press, Cambridge, Cambridge Univ, pp. 105–149.
Bohm, E., Lippold, J., Gutjahr, M., Frank, M., Blaser, P., Antz, B., Fohlmeister, J., Frank, N., Andersen, M.B., Deininger, M., 2015. Strong and deep Atlantic meridional overturning circulation during the last glacial cycle. Nature 517 (7532), 73–76.
Bond, G., Broecker, W., Johnsen, S., McManus, J., Labeyrie, L., Jouzel, J., Bonani, G., 1992. Correlations between climate records from North Atlantic sediments and Greenland ice. Nature 365, 143–147. https://doi.org/10.1038/365143a0.
Bond, G., Showers, W., Cheseby, M., Lotti, R., Almasi, P., deMenocal, P., Priore, P., Cullen, H., Hajdas, I., Bonani, G., 1997. A pervasive millennial-scale cycle in North Atlantic Holocene and glacial climates. Science 278, 1257–1266.
Bond, G., Kromer, B., Beer, J., Muscheler, R., Evans, M., Showers, W., Hoffmann, S., Lotti-Bond, R., Hajdas, I., Bonani, G., 2001. Persistent solar influence on North Atlantic climate during the Holocene. Science 294, 2130–2136. https://doi.org/10.1126/science.1065680.
Boswell, S.M., Toucanne, S., Pitel-Roudaut, M., Creyts, T.T., Eynaud, F., Bayon, G., 2019. Enhanced surface melting of the Fennoscandian Ice Sheet during periods of North Atlantic cooling. Geology 47 (7), 664–668. https://doi.org/10.1130/g46370.1.
Cacho, I., Grimalt, J.O., Pelejero, C., Canals, M., Sierro, F.J., Flores, J.A., Shackleton, N., 1999. Dansgaard-oeschger and Heinrich event imprints in Alboran Sea paleotemperatures. Paleoceanography 14, 698–705. https://doi.org/10.1029/1999pa900044.
Cayre, O., Lancelot, Y., Vincent, E., Hall, M.A., 1999. Paleoceanographic reconstructions from planktonic foraminifera off the Iberian margin: temperature, salinity, and Heinrich events. Paleoceanography 14, 384–396.
Channell, J.E.T., Hodell, D.A., 2013. Magnetic signatures of Heinrich-like detrital layers in the Quaternary of the North Atlantic. Earth Planet. Sci. Lett. 369, 260–270.
Channell, J.E.T., Hodell, D.A., Romero, O., Hillaire-Marcel, C., de Vernal, A., Stoner, J.S., Mazaud, A., Röhl, U., 2012. A 750-kyr detrital-layer stratigraphy for the North Atlantic (IODP Sites U1302–U1303, Orphan Knoll, Labrador Sea). Earth Planet. Sci. Lett. 317–318, 218–230. https://doi.org/10.1016/j.epsl.2011.11.029.
Chapman, M.R., 2010. Seasonal production patterns of planktonic foraminifera in the NE Atlantic Ocean: Implications for paleotemperature and hydrographic reconstructions. Paleoceanography 25, PA1101. https://doi.org/10.1029/2008PA001708.
Cheng, H., Edwards, R.L., Broecker, W.S., Denton, G.H., Kong, X., Wang, Y., Zhang, R., Wang, X., 2009. Ice age terminations. Science 326 (5950), 248–252.
Clark, P.U., McCabe, A.M., Mix, A.C., Weaver, A.J., 2004. Rapid rise of sea level 19,000 years ago and its global implications. Science 304 (5674), 1141–1144.
Costas, S., Naughton, F., Goble, R., Hans, R., 2016. Windiness spells in SW Europe since the last glacial maximum. Earth & Planetary Science Letters 436, 82–92.
Coste, B., Fiúza, A.F.G., Minas, H.-J., 1986. Conditions hydrologiques et chimiques associées à l'upwelling côtier du Portugal en fin d'été. Oceanol. Acta 9, 149–158.
Couchoud, I., Genty, D., Hoffmann, D., Drysdale, R., Blamart, D., 2009. Millennial-scale climate variability during the last Interglacial recorded in a speleothem from South-Western France. Quat. Sci. Rev. 28, 3263–3274.
Cutmore, A., Ausín, B., Maslin, M., Eglinton, T., Hodell, D., Muschitiello, F., Menviel, L., Haghipour, N., Martrat, B., Margari, V., Tzedakis, P.C., 2021. Abrupt intrinsic and extrinsic responses of southwestern Iberian vegetation to millennial-scale variability over the past 28 ka. J. Quat. Sci. https://doi.org/10.1002/jqs.3392.
de Abreu, L., Shackleton, N.J., Schönfeld, J., Hall, M.A., Chapman, M., 2003. Millennial-scale oceanic climate variability off the western Iberian margin during the last two glacial periods. Mar. Geol. 196, 1–20.
de Abreu, L., Abrantes, F., Shackleton, N.J., Tzedakis, P.C., McManus, J.F., Oppo, D.W., Hall, M.A., 2005. Ocean climate variability in the eastern North Atlantic during interglacial marine isotope stage 11: a partial analogue to the Holocene? Paleoceanography 20, PA3009.
deMenocal, P., Ortiz, J., Guilderson, T., Adkins, J., Sarnthein, M., Baker, L., Yarusinsky, M., 2000. Abrupt onset and termination of the African Humid Period: rapid climate responses to gradual insolation forcing. Quat. Sci. Rev. 19, 347–361.
Denton, G.H., Anderson, R.F., Toggweiler, J.R., Edwards, R.L., Schaefer, J.M., Putnam, A. E., 2010. The last glacial termination. Science 328 (5986), 1652–1656.
Drysdale, R.N., Zanchetta, G., Hellstrom, J.C., Zhao, J.-X., Fallick, A., Isola, I., Bruschi, G., 2004. Palaeoclimatic implications of the growth history and stable isotope ($\delta^{18}O$ and $\delta^{13}C$) geochemistry of a middle to late Pleistocene stalagmite from Central-Western Italy. Earth Planet. Sci. Lett. 227, 215–229.
Drysdale, R.N., Zanchetta, G., Hellstrom, J., Fallick, A., Zhao, J.-X., 2005. Stalagmite evidence for the onset of the last Interglacial in southern Europe at 129 ± 1 ka. Geophys. Res. Lett. 32, L24708.
Duan, W., Cheng, H., Tan, M., Ma, Z., Chen, S., Wang, L., Wang, X., Cui, L., 2022. Structural similarity between termination III and I. Quat. Sci. Rev. 296, 107808.
Ehlers, J., Gibbard, P.L., Hughes, P.D., 2011. Developments in Quaternary Sciences, vol. 15. Elsevier.
Ellison, C.R.W., Chapman, M.R., Hall, I.R., 2006. Surface and deep ocean interaction during the cold climate event 8200 years ago. Science 312, 1929–1932.
Site U1385. In: Expedition 339 Scientists, Stow, D.A.V., Hernández-Molina, F.J., Alvarez Zarikian, C.A. (Eds.), 2013. the Expedition 339 Scientists (Eds.), Proc. IODP 339. Integrated Ocean Drilling Program Management International, Inc., Tokyo.
Eynaud, F., Turon, J.L., Sanchez-Goni, M.F., Gendreau, S., 2000. Dinoflagellate cyst evidence of 'Heinrich-like events' off Portugal during the Marine Isotopic Stage 5. Mar. Micropaleontol. 40, 9–21. https://doi.org/10.1016/S0377-8398(99)00045-6.
Eynaud, F., de Abreu, L., Voelker, A., Schonfeld, J., Salgueiro, E., Turon, J.L., Penaud, A., Toucanne, S., Naughton, F., Sanchez-Goni, M.F., Malaize, B., Cacho, I., 2009. Position of the polar front along the western Iberian margin during key cold episodes of the last 45 ka. Geochem. Geophys. Geosyst. 10, Q07U05. https://doi.org/10.1029/2009GC002398.
Ezat, M.M., Rasmussen, T.L., Groeneveld, J., 2014. Persistent intermediate water warming during cold stadials in the southeastern Nordic seas during the past 65 k.y. Geology 42 (8), 663–666. https://doi.org/10.1130/g35579.1.
Fiúza, A.F.G., 1983. Upwelling patterns off Portugal. In: Suess, E., Thiede, J. (Eds.), Coastal Upwelling its Sediment Record. Plenum Press, New York, pp. 85–98.
Fiúza, A.F.G., Hamann, M., Ambar, I., Diaz del Rio, G., Gonzalez, N., Cabanas, J.M., 1998. Water masses and their circulation off western Iberia during May 1993. Deep Sea Res Part I: Oceanogr. Res. Pap. 45, 1127–1160.
Fronval, T., Jansen, E., Haflidason, H., Sejrup, H.P., 1998. Variability in surface and deep water conditions in the Nordic seas during the last interglacial period. Quat. Sci. Rev. 17 (9–10), 963–985.
Galaasen, E.V., Ninnemann, U.S., Kessler, A., Irvalı, N., Rosenthal, Y., Tjiputra, J., Bouttes, N., Roche, D., Kleiven, H., Hodell, D.A., 2020. Interglacial instability of North Atlantic deep water ventilation. Science 367 (6485), 1485–1489.
González-Lanchas, A., Flores, J.A., Sierro, F.J., Sánchez-Goñi, M.F., Rodrigues, T., Ausín, B., Oliveira, D., Naughton, F., Marino, M., Maiorano, P., Balestra, B., 2021. Control mechanisms of primary productivity revealed by calcareous nannoplankton from marine isotope stages 12 to 9 at the Shackleton Site (IODP Site U1385). Paleoceanography and Paleoclimatology 36 (2021PA004246).
Grant, K.M., Rohling, E.J., Bar-Matthews, M., Ayalon, A., Medina-Elizalde, M., Ramsey, C., Satow, C., Roberts, A.P., 2012. Rapid coupling between ice volume and polar temperature over the past 150 kyr. Nature 491, 744–747.
Grunert, P., Skinner, L., Hodell, D.A., Piller, W.E., 2015. A micropalaeontological perspective on export productivity, oxygenation and temperature in NE Atlantic deep-waters across Terminations I and II. Glob. Planet. Chang. 131, 174–191.
Hall, I.R., Moran, S.B., Zahn, R., Knutz, P.C., Shen, C.C., Edwards, R.L., 2006. Accelerated drawdown of meridional overturning in the late-glacial Atlantic triggered by transient pre-H event freshwater perturbation. Geophys. Res. Lett. 33 (16).
Henry, L.G., McManus, J.F., Curry, W.B., Roberts, N.L., Piotrowski, A.M., Keigwin, L.D., 2016. North Atlantic Ocean circulation and abrupt climate change during the last glaciation. Science 353, 470–474.
Hodell, D.A., Channell, J.E., Curtis, J.H., Romero, O.E., Röhl, U., 2008. Onset of "Hudson Strait" Heinrich events in the eastern North Atlantic at the end of the middle Pleistocene transition (~ 640 ka)? Paleoceanography 23 (4), PA4218.
Hodell, D.A., Crowhurst, S., Lourens, L., Margari, V., Nicolson, J., Rolfe, J.E., Skinner, L. C., Thomas, N., Tzedakis, P.C., Mleneck-Vautravers, M.J., Wolff, E.W.A., 2023. 1.5-Million- Year Record of Orbital and Millennial Climate Variability in the North Atlantic. Clim. Past 19, 607–636. https://doi.org/10.5194/cp-2022-61.
Hodell, D.A., Lourens, L., Crowhurst, S., Konijnendijk, T., Tjallingii, R., the Shackleton Site Project Members, 2015. A reference time scale for Site U1385 (Shackleton Site) on the Iberian margin. Glob. Planet. Chang. 133, 49–64.
Hodell, D.A., Nicholl, J.A., Bontognali, T.R.R., Danino, S., Dorador, J., Dowdeswell, J.A., Einsle, J., Kuhlmann, H., Martrat, B., Mleneck-Vautravers, M.J., Rodríguez-Tovar, F. J., Röhl, U., 2017. Anatomy of Heinrich Layer 1 and its role in the last deglaciation. Paleoceanography 32 (3), 284–303. https://doi.org/10.1002/2016pa003028.
Hughes, P.D., Gibbard, P.L., 2018. Global glacier dynamics during 100 ka Pleistocene glacial cycles. Quat. Res. 90 (1), 222–243.
Husum, K., Hald, M., 2012. Arctic planktic foraminiferal assemblages: Implications for subsurface temperature reconstructions. Mar. Micropaleontol. 96, 38–47.
Huybers, P., 2006. Early Pleistocene glacial cycles and the integrated summer insolation forcing. Science 313, 5786. https://doi.org/10.1126/science.1125249.
Incarbona, A., Martrat, B., Di Stefano, E., Grimalt, J.O., Pelosi, N., Patti, B., Tranchida, G., 2010. Primary productivity variability on the Atlantic Iberian Margin over the last 70,000 years: evidence from coccolithophores and fossil organic compounds. Paleoceanography 25 (2), PA2218. https://doi.org/10.1029/2008pa001709.
Ivanovic, R.F., Gregoire, L.J., Burke, A., Wickert, A.D., Valdes, P.J., Ng, H.C., Robinson, L., McManus, J., Mitrovica, J., Lee, L., Dentith, J., 2018. Acceleration of northern ice sheet melt induces AMOC slowdown and northern cooling in

simulations of the early last deglaciation. Paleoceanography and Paleoclimatology 33 (7), 807–824.
Jiang, N., Yan, Q., 2020. Evolution of the meridional shift of the subtropical and subpolar westerly jet over the Southern Hemisphere during the past 21,000 years. Quat. Sci. Rev. 246, 106544.
Jiménez-Amat, P., Zahn, R., 2015. Offset timing of climate oscillations during the last two glacial-interglacial transitions connected with large-scale freshwater perturbation. Paleoceanography 30, 768–788.
Johannessen, T., Jansen, E., Flatoy, A., Ravelo, A.C., 1994. In: Zahn, R., Pedersen, T.F., Kanimski, M.A., Labeyrie, L. (Eds.), The relationship between surface water masses, oceanographic fronts and paleoclimatic proxies in surface sediments of the Greenland, Iceland, Norwegian seas, NATO ASI Series, 117. Springer-Verlag, New York, pp. 61–85.
Jouzel, J., Masson-Delmotte, V., Cattani, O., Dreyfus, G., Falourd, S., Hoffmann, G., Minster, B., Nouet, J., Barnola, J.M., Chappellaz, J., Fischer, H., 2007. Orbital and millennial Antarctic climate variability over the past 800,000 years. Science 317 (5839), 793–796.
Kaboth-Bahr, S., Bahr, A., Zeeden, C., Toucanne, S., Eynaud, F., Jiménez-Espejo, F., Röhl, U., Friedrich, O., Pross, J., Löwemark, L., Lourens, L.J., 2018. Monsoonal forcing of European ice-sheet dynamics during the late Quaternary. Geophysical Res. Letters 45, 7066–7074.
Kennett, J.P., Srinivasan, M.S., 1983. Neogene Planktonic Foraminifera. A Phylogenetic Atlas. Hutchinson Ross Publishing Company, New York.
Kleiven, H.F., Kissel, C., Laj, C., Ninnemann, U., Richter, T., Cortijo, E., 2008. Reduced North Atlantic deep water coeval with the glacial Lake Agassiz freshwater outburst. Science 319, 60–64. https://doi.org/10.1126/science.1148924.
Köhler, P., Nehrbass-Ahles, C., Schmitt, J., Stocker, T.F., Fischer, H., 2017. A 156 kyr smoothed history of the atmospheric greenhouse gases CO2, CH4, and N2O and their radiative forcing. Earth Syst. Sci. Data 9, 363–387. https://doi.org/10.5194/essd-9-363-2017.
Kroon, D., Ganssen, G., 1988. Northern Indian Ocean upwelling cells and the stable isotope composition of living planktic foraminifers. In: Brummer, G.J.A., Kroon, D. (Eds.), Planktonic Foraminifers as Tracers of Ocean-Climate History. Free University Press, Amsterdam, pp. 299–317.
Kucera, M., Rosell-Mele, A., Schneider, R., Waelbroeck, C., Weinelt, M., 2005. Multiproxy approach for the reconstruction of the glacial ocean surface (MARGO). Quat. Sci. Rev. 24, 813–819.
Landais, A., Capron, E., Masson-Delmotte, V., Toucanne, S., Rhodes, R., Popp, T., Vinther, B., Minster, B., Prié, F., 2018. Ice core evidence for decoupling between midlatitude atmospheric water cycle and Greenland temperature during the last deglaciation. Clim. Past 14 (10), 1405–1415.
Lang, N., Wolff, E.W., 2011. Interglacial and glacial variability from the last 800 ka in marine, ice and terrestrial archives. Clim. Past 7 (2), 361–380.
Laskar, J., Fienga, A., Gastineau, M., Manche, H., 2011. La2010: a new orbital solution for the long-term motion of the Earth. Astronomy & Astrophysics 532, A89.
Lebreiro, S., Moreno, J., McCave, I., Weaver, P., 1996. Evidence for Heinrich layers off Portugal (Tore Seamount: 39 N, 12 W). Mar. Geol. 131, 47–56.
Lebreiro, S.M., Moreno, J.C., Abrantes, F.F., Pflaumann, U., 1997. Productivity and paleoceanographic implications on the Tore Seamount (Iberian margin) during the last 225 kyr: foraminiferal evidence. Paleoceanography 12, 718–727.
Locarnini, R.A., Mishonov, A.V., Antonov, J.I., Boyer, T.P., Garcia, H.E., Baranova, O.K., Zweng, M.M., Johnson, D.R., 2010. World Ocean Atlas 2009, volume 1: Temperature. In: Levitus, S. (Ed.), NOAA Atlas NESDIS 68. U. S. Government Printing Office, Washington, D.C.
Marcott, S.A., Clark, P., Padman, L., Klinkhammer, G., Springer, S., Liu, Z., Otto-Bliesner, B., Carlson, A., Ungerer, A., Padman, J., He, F., Cheng, J., Schmittner, A., 2011. Ice-shelf collapse from subsurface warming as a trigger for Heinrich events. Proc. Nat. Acad. Sci. 108, 13415–13419. https://doi.org/10.1073/pnas.1104772108.
Margari, V., Skinner, L.C., Hodell, D.A., Martrat, B., Toucanne, S., Grimalt, J.O., Gibbard, P.L., Lunkka, J.P., Tzedakis, P.C., 2014. Land-ocean changes on orbital and millennial time scales and the penultimate glaciation. Geology 42, 183–186. https://doi.org/10.1130/G35070.1.
Martin-Garcia, G.M., Alonso-Garcia, M., Sierro, F.J., Hodell, D.A., Flores, J.A., 2015. Severe cooling episodes at the onset of deglaciations on the Southwestern Iberian margin from MIS 21 to 13 (IODP site U1385). Glob. Planet. Change 135, 159–169.
Martins, M.V.A., Rey, D., Pereira, E., Plaza-Morlote, M., Salgueiro, E., Moreno, J., Duleba, W., Ribeiro, S., dos Santos, J.F., Dardon, U., Bernabeu, A., 2018. Influence of dominant wind patterns in a distal region of the NW Iberian margin during the last glaciation. J. Geol. Soc. 175 (2), 321–335.
Martrat, B., Grimalt, J.O., Shackleton, N.J., de Abreu, L., Hutterli, M.A., Stocker, T.F., 2007. Four climate cycles of recurring deep and surface water destabilizations on the Iberian margin. Science 317, 502–507.
Martrat, B., Jimenez-Amat, P., Zahn, R., Grimalt, J.O., 2014. Similarities and dissimilarities between the last two deglaciations and interglaciations in the North Atlantic region. Quat. Sci. Rev. 99, 122–134.
Max, L., Nürnberg, D., Chiessi, C.M., Lenz, M.M., Mulitza, S., 2022. Subsurface Ocean warming preceded Heinrich events. Nat. Commun. 13 (1), 1–8.
McCartney, M.S., Talley, L.D., 1982. The subpolar mode water of the North Atlantic Ocean. J. Phys. Oceanogr. 12, 1169–1188.
McManus, J.F., Oppo, D.W., Cullen, J.L., 1999. A 0.5-million-year record of millennial-scale climate variability in the North Atlantic. Science 283 (5404), 971–975.
McManus, J.F., Francois, R., Gherardi, J.M., Keigwin, L.D., Brown-Leger, S., 2004. Collapse and rapid resumption of Atlantic meridional circulation linked to deglacial climate changes. Nature 428 (6985), 834–837.
Menviel, L., Spence, P., Yu, J., Chamberlain, M.A., Matear, R.J., Meissner, K.J., England, M.H., 2018. Southern Hemisphere westerlies as a driver of the early deglacial atmospheric CO2 rise. Nat. Commun. 9 (1), 1–12.
Milner, A.M., Müller, U.C., Roucoux, K.H., Collier, R.E.L., Pross, J., Kalaitzidis, S., Christanis, K., Tzedakis, P.C., 2013. Environmental variability during the Last Interglacial: a new high- resolution pollen record from Tenaghi Philippon, Greece. *J. Quat. Sci.* 28, 113–117.
Monnin, E., Indermuhle, A., Dallenbach, A., Fluckiger, J., Stauffer, B., Stocker, T.F., Raynaud, D., Barnola, J.M., 2001. Atmospheric CO2 concentrations over the last glacial termination. Science 291 (5501), 112–114.
Moreno, A., Stoll, H.M., Jimenez-Sanchez, M., Cacho, I., Valero-Garces, B., Ito, E., Edwards, L.R., 2010. A speleothem record of rapid climatic shifts during last glacial period from Northern Iberian Peninsula. Glob. Planet. Chang. 71, 218–231.
Morrill, C., LeGrande, A.N., Renssen, H., Bakker, P., Otto-Bliesner, B.L., 2013. Model sensitivity to North Atlantic freshwater forcing at 8.2 ka. Clim. Past 9, 955–968.
Moseley, G.E., Spotl, C., Cheng, H., Boch, R., Min, A., Edwards, R.L., 2015. Termination-II interstadial/stadial climate change recorded in two stalagmites from the north European Alps. Quat. Sci. Rev. 127, 229–239.
Naafs, B.D.A., Hefter, J., Grützner, J., Stein, R., 2013. Warming of surface waters in the mid- latitude North Atlantic during Heinrich events. Paleoceanography 28, 153–163.
Naughton, F., Goni, M.F.S., Desprat, S., Turon, J.L., Duprat, J., Malaize, B., Joli, C., Cortijo, E., Drago, T., Freitas, M.C., 2007. Present-day and past (last 25 000 years) marine pollen signal off western Iberia. Mar. Micropaleontol. 62, 91–114.
Naughton, F., Goñi, M.F.S., Kageyama, M., Bard, E., Duprat, J., Cortijo, E., Desprat, S., Malaizé, B., Joly, C., Rostek, F., Turon, J.L., 2009. Wet to dry climatic trend in North-Western Iberia within Heinrich events. Earth Planet. Sci. Lett. 284 (3–4), 329–342.
Naughton, F., Sanchez-Goni, M.F., Rodrigues, T., Salgueiro, E., Costas, S., Desprat, S., Duprat, J., Michel, E., Rossignol, L., Zaragosi, S., Voelker, A.H.L., Abrantes, F., 2015. Climate variability across the last deglaciation in NW Iberia and its margin. Quat. Int. 414, 9–22.
Nave, S., Lebreiro, S., Michel, E., Kissel, C., Figueiredo, M.O., Guihou, A., Ferreira, A., Labeyrie, L., Alberto, A., 2018. The Atlantic meridional overturning circulation as productivity regulator of the North Atlantic subtropical Gyre. Quat. Res. 91, 399–413.
North Greenland Ice Core Project members, 2004. High-resolution record of Northern Hemisphere climate extending into the last interglacial period. Nature 431, 147–151.
Obrochta, S.P., Crowley, T.J., Channell, J.E., Hodell, D.A., Baker, P.A., Seki, A., Yokoyama, Y., 2014. Climate variability and ice-sheet dynamics during the last three glaciations. Earth Planet. Sci. Lett. 406, 198–212.
Oliveira, D., Desprat, S., Yin, Q., Naughton, F., Trigo, R., Rodrigues, T., Abrantes, F., Sanchez- Goñi, M.F., 2018. Unravelling the forcings controlling the vegetation and climate of the best orbital analogues for the present interglacial in SW Europe. Clim. Dyn. 51, 667–686.
Olson, H.C., Smart, C.W., 2004. Pleistocene climatic history reflected in planktonic foraminifera from ODP Site 1073 (Leg 174A), New Jersey margin, NW Atlantic Ocean. Marine Micropaleontology 51 (3–4), 213–238. https://doi.org/10.1016/j.marmicro.2003.11.002.
Oppo, D.W., McManus, J.F., Cullen, J.L., 2003. Deepwater variability in the Holocene epoch. Nature 422 (6929), 277.
Oppo, D.W., McManus, J.F., Cullen, J.L., 2006. Evolution and demise of the last Interglacial warmth in the subpolar North Atlantic. Quat. Sci. Rev. 25 (23–24), 3268–3277.
Ottens, J.J., 1992. Planktic Foraminifera as Indicators of Ocean Environments in the Northeast Atlantic (Ph. D. thesis). University of Amsterdam, Amsterdam.
Palumbo, E., Flores, J.A., Perugia, C., Emanuele, D., Petrillo, Z., Rodrigues, T., Voelker, A.H.L., Amore, F.O., 2013. Abrupt variability of the last 24 ka recorded by coccolithophore assemblages off the Iberian margin (core MD03-2699). Journal of Quat. Sci. 28, 320–328.
Palumbo, E., Voelker, A.H.L., Flores, J.A., Amore, O.F., 2018. Surface-ocean dynamics during eccentricity minima: a comparison between interglacial Marine Isotope Stage (MIS) 1 and MIS 11 on the Iberian margin. Glob. Planet. Chang. 172, 242–255.
Past Interglacials Working Group, 2015. Interglacials of the last 800,000 years. Rev. Geophys. 54, 162–219. https://doi.org/10.1002/2015RG000482.
Peck, V.L., Hall, I.R., Zahn, R., Elderfield, H., Grousset, F., Hemming, S.R., Scourse, J.D., 2006. High resolution evidence for linkages between NW European ice sheet instability and Atlantic Meridional Overturning Circulation. Earth Planet. Sci. Lett. 243 (3–4), 476–488. https://doi.org/10.1016/j.epsl.2005.12.023.
Peliz, A., Dubert, J., Santos, A.M.P., Oliveira, P.B., Le Cann, B., 2005. Winter upper ocean circulation in the Western Iberian Basin: Fronts, Eddies and Poleward Flows: an overview. Deep-Sea Res. Pt I 52, 621–646.
Perez-Mejías, C., Moreno, A., Sancho, C., Bartolome, M., Stoll, H., Cacho, I., Cheng, H., Edwards, R.L., 2017. Abrupt climate changes during termination III in southern Europe. Proc. Natl. Acad. Sci. 114, 10047–10052.
Pflaumann, U., Dupratm, J., Pujol, C., Labeyrie, L.D., 1996. SIMMAX: a modern analog technique to deduce Atlantic Sea surface temperatures from planktonic Foraminifera in deep-sea sediments. Paleoceanography 11, 15–35.
Pflaumann, U., Sarnthein, M., Chapman, M., de Abreu, L., Funnell, B., Huels, M., Kiefer, T., Maslin, M., Schulz, H., Swallow, J., van Kreveld, S., Vautravers, M., Vogelsang, E., Weinelt, M., 2003. Glacial North Atlantic: sea-surface conditions reconstructed by GLAMAP 2000. Paleoceanography 18, 1065. https://doi.org/10.1029/2002PA000774.
Pickarski, N., Litt, T., 2017. A new high-resolution pollen sequence at Lake Van, Turkey: insights into penultimate interglacial–glacial climate change on vegetation history. Clim. Past 13 (6), 689–710.

Pinho, T.M., Chiessi, C.M., Portilho-Ramos, R.C., Campos, M.C., Crivellari, S., Nascimento, R.A., Albuquerque, A.L., Bahr, A., Mulitza, S., 2021. Meridional changes in the South Atlantic Subtropical Gyre during Heinrich Stadials. Sci. Rep. 11 (1), 1–10.
Pujol, C., 1980. Les foraminiferes planctoniques de l'Atlantique Nord au Quaternaire. Ecologie, Stratigraphie, Environnement. Ph.D. thesis, 254 pp. Univ. Bordeaux I, Bordeaux, France.
Railsback, L.B., Gibbard, P.L., Head, M.J., Voarintsoa, N.R.G., Toucanne, S., 2015. An optimized scheme of lettered marine isotope substages for the last 1.0 million years, and the climatostratigraphic nature of isotope stages and substages. Quat. Sci. Rev. 111, 94–106.
Regattieri, E., Zanchetta, G., Drysdale, R.N., Isola, I., Woodhead, J.D., Hellstrom, J.C., Giaccio, B., Greig, A., Baneschi, I., Dotsika, E., 2016. Environmental variability between the penultimate deglaciation and the mid Eemian: insights from Tana che Urla (Central Italy) speleothem trace element record. Quat. Sci. Rev. 152, 80–92.
Regattieri, E., Giaccio, B., Nomade, S., Francke, A., Vogel, H., Drysdale, R.N., Perchiazzi, N., Wagner, B., Gemelli, M., Mazzini, I., Boschi, C., Galli, P., Peronace, E., 2017. A last Interglacial record of environmental changes from the Sulmona Basin (Central Italy). Palaeogeogr. Palaeoclimatol. Palaeoecol. 472, 51–66. https://doi.org/10.1016/j.palaeo.2017.02.013.
Reißig, S., Nürnberg, D., Bahr, A., Poggemann, D.-W., Hoffmann, J., 2019. Southward displacement of the North Atlantic subtropical Gyre circulation system during North Atlantic cold spells. Paleoceanogr. Paleoclimatol. 34, 866–885.
Repschläger, J., Weinelt, M., Kinkel, H., Andersen, N., Garbe-Schönberg, D., Schwab, C., 2015. Response of the subtropical North Atlantic surface hydrography on deglacial and Holocene AMOC changes. Paleoceanography 30 (5), 456–476. https://doi.org/10.1002/2014PA002637.
Repschläger, J., Zhao, N., Rand, D., Lisiecki, L., Muglia, J., Mulitza, S., Schmittner, A., Cartapanis, O., Bauch, H.A., Schiebel, R., Haug, G.H., 2021. Active North Atlantic Deepwater formation during Heinrich Stadial 1. Quat. Sci. Rev. 270, 107–145.
Roche, D.M., Wiersma, A.P., Renssen, H., 2010. A systematic study of the impact of freshwater pulses with respect to different geographical locations. Clim. Dyn. 34, 997–1013.
Rodrigues, T., Voelker, A., Grimalt, J., Abrantes, F., Naughton, F., 2011. Iberian margin sea surface temperature during MIS 15 to 9 (580–300 ka): Glacial suborbital variability versus interglacial stability. Paleoceanography 26, PA1204.
Rohling, E., Palike, H., 2005. Centennial-scale climate cooling with a sudden cold event around 8,200 years ago. Nature 434, 975–979.
Roucoux, K., Tzedakis, C., Frogley, M., Lawson, I., Preece, R., 2008. Vegetation history of the marine isotope stage 7 interglacial complex at Ioannina, NW Greece. Quat. Sci. Rev. 27, 1378–1395. https://doi.org/10.1016/j.quascirev.2008.04.002.
Sadori, L., Koutsodendris, A., Panagiotopoulos, K., Masi, A., Bertini, A., Combourieu-Nebout, N., Francke, A., Kouli, K., Joannin, S., Mercuri, A.M., Peyron, O., Torri, P., Wagner, B., Zanchetta, G., Sinopoli, G., Donders, T.H., 2016. Pollen-based paleoenvironmental and paleoclimatic change at Lake Ohrid (South-Eastern Europe) during the past 500 ka. Biogeosciences 13, 1423–1437. https://doi.org/10.5194/bg-13-1423-2016.
Salgueiro, E., Voelker, A., Abrantes, F., Meggers, H., Pflaumann, U., Loncaric, N., Gonzalez- Alvarez, R., Oliveira, P., Bartels-Jonsdottir, H., Moreno, J., Wefer, G., 2008. Planktonic foraminifera from modern sediments reflect upwelling patterns off Iberia: Insights from a regional transfer function. Mar. Micropaleontol. 66, 135–164.
Salgueiro, E., Voelker, A.H.L., de Abreu, L., Abrantes, F., Meggers, H., Wefer, G., 2010. Temperature and productivity changes off the western Iberian margin during the last 150 ky. Quat. Sci. Rev. 29, 680–695.
Salgueiro, E., Naughton, F., Voelker, A.H.L., de Abreu, L., Alberto, A., Rossignol, L., Duprat, J., Magalhães, V.H., Vaqueiro, S., Turon, J.L., Abrantes, F., 2014. Past circulation along the western Iberian margin: a time slice vision from the last Glacial to the Holocene. Quat. Sci. Rev. 106, 316–329.
Salgueiro, E., Voelker, A.H.L., Martin, P.A., Rodrigues, T., Zúñiga, D., Froján, M., de la Granda, F., Villacieros-Robineau, N., Alonso-Pérez, F., Alberto, A., Rebotim, A., González-Álvarez, R., Castro, C.G., Abrantes, F., 2020. $\delta^{18}O$ and Mg/Ca thermometry in planktonic foraminifera: a multiproxy approach toward tracing coastal upwelling dynamics. Paleoceanography and Paleoclimatology 35. https://doi.org/10.1029/2019PA003726, 2019PA003726.
Sanchez-Goñi, M., Eynaud, F., Turon, J.L., Shackleton, N.J., 1999. High resolution palynological record off the Iberian margin: direct land-sea correlation for the last Interglacial complex. Earth Planet. Sci. Lett. 171 (1), 123–137.
Schiebel, R., Hemleben, C., 2000. Interannual variability of planktic foraminiferal populations and test flux in the eastern North Atlantic Ocean (JGOFS). Deep-Sea Research Part II—Topical Studies Oceanography 47, 1809–1852.
Schiebel, R., Hemleben, C., 2017. Planktic Foraminifers in the Modern Ocean. https://doi.org/10.1007/978-3-662-50297-6.
Schiebel, R., Waniek, J., Bork, M., Hemleben, C., 2001. Planktic foraminiferal production stimulated by chlorophyll redistribution and entrainment of nutrients. Deep-Sea Research Part I- Oceanographic Research Papers 48, 721–740.
Schlitzer, R., 2014. Ocean Data View. http://odv.awi.de.
Schmittner, A., Lund, D.C., 2015. Early deglacial Atlantic overturning decline and its role in atmospheric CO2 rise inferred from carbon isotopes (δ13C). Clim. Past 11 (2), 135–152.
Schmuker, B., Schiebel, R., 2002. Planktic foraminifers and hydrography of the eastern and northern Caribbean Sea. Mar. Micropaleontol. 46, 387–403.
Schwab, C., Kinkel, H., Weinelt, M., Repschlager, J., 2012. Coccolithophore paleoproductivity and ecology response to deglacial and Holocene changes in the Azores Current System. Paleoceanography 27, PA3210.
Shackleton, N.J., 2000. The 100,000-year ice-age cycle identified and found to lag temperature, carbon dioxide, and orbital eccentricity. Science 289, 1897–1902.
Shaffer, G., Olsen, S.M., Bjerrum, C.J., 2004. Ocean subsurface warming as a mechanism for coupling Dansgaard-Oeschger climate cycles and ice-rafting events. Geophys. Res. Lett. 31 (24), L24202. https://doi.org/10.1029/2004gl020968.
Shakun, J.D., Clark, P.U., He, F., Marcott, S.A., Mix, A.C., Liu, Z., Otto-Bliesner, B., Schmittner, A., Bard, E., 2012. Global warming preceded by increasing carbon dioxide concentrations during the last deglaciation. Nature 484 (7392), 49–54.
Shakun, J.D., Lea, D.W., Lisiecki, L.E., Raymo, M.E., 2015. An 800-kyr record of global surface ocean δ18O and implications for ice volume-temperature coupling. Earth Planet. Sci. Lett. 426, 58–68.
Sierro, F.J., Hodell, D.A., Andersen, N., Azibeiro, L.A., Jimenez-Espejo, F.J., Bahr, A., Flores, J.A., Ausin, B., Rogerson, M., Lozano-Luz, R., Lebreiro, S.M., 2020. Mediterranean overflow over the last 250 kyr: freshwater forcing from the tropics to the ice sheets. Paleoceanography and Paleoclimatology 35 (9) (2020PA003931).
Singh, A.D., Verma, K., Jaiswal, S., Alonso-Garcia, M., Li, B., Abrantes, F., 2015. Planktic foraminiferal responses to orbital scale oceanographic changes off the western Iberian margin over the last 900 kyr: results from IODP site U1391. Glob. and Plan. Chan. 135, 47–56.
Skinner, L.C., Shackleton, N.J., 2006. Deconstructing terminations I and II: revisiting the glacioeustatic paradigm based on deep-water temperature estimates. Quat. Sci. Rev. 25, 3312–3321.
Sousa, F.M., Bricaud, A., 1992. Satellite-derived phytoplankton pigment structures in the Portuguese upwelling area. Journal of Geophysical Research: Oceans 97 (C7), 11343–11356.
Spezzaferri, S., Kucera, M., Pearson, P.N., Wade, B.S., Rappo, S., Poole, C.R., Morard, R., Stalder, C., 2015. Fossil and Genetic evidence for the Polyphyletic Nature of the Planktonic Foraminifera "Globigerinoides", and Description of the New Genus Trilobatus. PLoS One 10 (5), 0128108. https://doi.org/10.1371/journal.pone.0128108.
Stoll, H.M., Cacho, I., Gasson, E., Sliwinski, J., Kost, O., Moreno, A., Iglesias, M., Torner, J., Perez- Mejias, C., Haghipour, N., Cheng, H., Edwards, R.L., 2022. Rapid northern hemisphere ice sheet melting during the penultimate deglaciation. Nat. Commun. 13, 3819. https://doi.org/10.1038/s41467-022-31619-3.
Storz, D., Schulz, H., Joanna, J., Waniek, D., Schulz-Bull, E., Kučera, M., 2009. Seasonal and interannual variability of the planktic foraminiferal flux in the vicinity of the Azores current. Deep-Sea Res. I Oceanogr. Res. Pap. 56 (1), 107–124.
Stríkis, N.M., Chiessi, C.M., Cruz, F.W., Vuille, M., Cheng, H., de Souza Barreto, E.A., Mollenhauer, G., Kasten, S., Karmann, I., Edwards, R.L., Bernal, J.P., 2015. Timing and structure of Mega-SACZ events during Heinrich Stadial 1. Geophys. Res. Lett. 42 (13), 5477–5484A.
Teles-Machado, A., Peliz, Á., McWilliams, J.C., Cardoso, R.M., Soares, P.M.M., Miranda, P.M.A., 2015. On the year-to-year changes of the Iberian Poleward current. J. Geophys. Res. Oceans 120, 4980–4999. https://doi.org/10.1002/2015JC010758.
Telford, R.J., Li, C., Kucera, M., 2013. Mismatch between the depth habitat of planktonic foraminifera and the calibration depth of SST transfer functions may bias reconstructions. Clim. Past 9 (2), 859–870.
Thomson, J., Nixon, S., Summerhayes, C.P., Rohling, E.J., Schonfeld, J., Zahn, R., Grootes, P., Abrantes, F., Gaspar, L., Vaqueiro, S., 2000. Enhanced productivity on the Iberian margin during glacial/interglacial transitions revealed by barium and diatoms. J. Geol. Soc. 157, 667–677.
Thunell, R.C., Sautter, L.R., 1992. Planktonic foraminiferal fauna and stable isotopic indices of upwelling: A sediment trap study in the San Pedro Basin, southern California. In: Summerhayes, C.P., Prell, W.L., Emeis, K.C. (Eds.), Upwelling Systems: Evolution since the Early Miocene, Geological Society Special Publication, vol. 64, pp. 77–91.
Toggweiler, J.R., Russell, J.L., Carson, S.R., 2006. Midlatitude westerlies, atmospheric CO2, and climate change during the ice ages. Paleoceanography 21 (2).
Toucanne, S., Zaragosi, S., Bourillet, J.F., Cremer, M., Eynaud, F., Van Vliet-Lanoë, B., Penaud, A., Fontanier, C., Turon, J.L., Cortijo, E., Gibbard, P.L., 2009. Timing of massive "Fleuve manche" discharges over the last 350 kyr: insights into the European ice-sheet oscillations and the European drainage network from MIS 10 to 2. Quat. Sci. Rev. 28, 1238–1256.
Toucanne, S., Zaragosi, S., Bourillet, J.F., Marieu, V., Cremer, M., Kageyama, M., Vliet-Lanoë, B.V., Eynaud, F., Turon, J.L., Gibbard, P.L., 2010. The first estimation of Fleuve Manche palaeoriver discharge during the last deglaciation: evidence for Fennoscandian ice sheet meltwater flow in the English Channel ca 20-18 ka ago. Ear. Planet. Sci. Lett. 290, 459–473.
Toucanne, S., Soulet, G., Freslon, N., Silva Jacinto, R., Dennielou, B., Zaragosi, S., Eynaud, F., Bourillet, J.F., Bayon, G., 2015. Millennial-scale fluctuations of the European Ice Sheet at the end of the last glacial, and their potential impact on global climate. Quat. Sci. Rev. 123, 113–133. https://doi.org/10.1016/j.quascirev.2015.06.010.
Tschumi, T., Joos, F., Gehlen, M., Heinze, C., 2011. Deep ocean ventilation, carbon isotopes, marine sedimentation and the deglacial CO2 rise. Clim. Past 7 (3), 771–800.
Turon, J.-L., Lézine, A.-M., Denèfle, M., 2003. Land–sea correlations for the last glaciation inferred from a pollen and dinocyst record from the portuguese margin. Quat. Res. 59 (1), 88–96. https://doi.org/10.1016/S0033-5894(02)00018-2.
Tzedakis, C., 2003. Timing and duration of last Interglacial conditions in Europe: a chronicle of a changing chronology. Quat. Sci. Rev. 22, 763–768.
Tzedakis, P.C., Drysdale, R.N., Margari, V., Skinner, L., Menviel, L., Rhodes, R., Taschetto, A., Hodell, D., Crowhurst, S., Hellstrom, J., Fallick, A.E., Toucanne, S., McManus, J., Martrat, B., Mokeddem, Z., Parrenin, F., Regattieri, E., Roe, K., Zanchetta, G., 2018. Enhanced climate instability in the North Atlantic and southern Europe during the last Interglacial. Nat. Commun. 9, 1–14.
Vautravers, M.J., Shackleton, N.J., 2006. Centennial-scale surface hydrology off Portugal during marine isotope stage 3: Insights from planktonic foraminiferal fauna

variability. Paleoceanography 21 (3), PA3004. https://doi.org/10.1029/2005pa001144.
Vautravers, M.J., Shackleton, N.J., Lopez-Martinez, C., Grimalt, J.O., 2004. Gulf Steam variability during marine isotope stage 3. Paleoeanography 19, PA2011.
Voelker, A.H.L., de Abreu, L., 2011. A Review of Abrupt Climate Change Events in the Northeastern Atlantic Ocean (Iberian Margin): Latitudinal, Longitudinal and Vertical Gradients. AGU Geophysical Monograph.
Voelker, A.H.L., Lebreiro, S.M., Schönfeld, J., Cacho, I., Erlenkeuser, H., Abrantes, F., 2006. Mediterranean outflow strengthening during northern hemisphere coolings: a salt source for the glacial Atlantic? Earth Planet. Sci. Lett. 245, 39–55.
Voelker, A.H.L., de Abreu, L., Schonfeld, J., Erlenkeuser, H., Abrantes, F., 2009. Hydrographic conditions along the Western Iberian margin during Marine isotope stage 2. Geochem. Geophys. Geosyst. 10, Q12U08. https://doi.org/10.1029/2009GC002605.
Wendt, K.A., Li, X., Edwards, R.L., Cheng, H., Spötl, C., 2021. Precise timing of MIS 7 substages from the Austrian Alps. Clim. Past 17 (4), 1443–1454.
Wilke, I., Meggers, H., Bickert, T., 2009. Depth habitats and seasonal distributions of recent planktic foraminifers in the Canary Islands region (29N) based on oxygen isotopes. Deep-Sea Res. I Oceanogr. Res. Pap. 56 (1), 89–106. https://doi.org/10.1016/j.dsr.2008.08.001.
Wolf, D., Kolb, T., Alcaraz-Castaño, M., Heinrich, S., Baumgart, P., Calvo, R., Sanchez, J., Ryborz, K., Schäfer, I., Bliedtner, M., Zech, R., Zöller, L., Faust, D., 2018. Climate deteriorations and Neanderthal demise in interior Iberia. Sci. Rep. 8, 1–10.
Wolf, D., Ryborz, K., Kolb, T., Calvo Zapata, R., Sanchez Vizcaino, J., Zöller, L., Faust, D., 2019. Origins and genesis of loess deposits in Central Spain, as indicated by heavy mineral compositions and grain-size variability. Sedimentology 66, 1139–1161.
Zhang, W., Wu, J., Wang, Y., Wang, Y., Cheng, H., Konga, X., Duan, F., 2014. A detailed East Asian monsoon history surrounding the 'Mystery Interval' derived from three Chinese speleothem records. Quat. Res. 82, 154–163. https://doi.org/10.1016/j.yqres.2014.01.010.
Ziemen, F.A., Kapsch, M.-L., Klockmann, M., Mikolajewicz, U., 2019. Heinrich events show two- stage climate response in transient glacial simulations. *Clim. Past.* 15, 153–168.